

THE SEARCH FOR AND STUDY
OF THE STRANGE MULTIBARYON STATES
IN SYSTEMS WITH Λ HYPERON
AND K_s^0 MESON IN pA COLLISION
AT MOMENTUM OF 10 GeV/c

*P. Zh. Aslanyan**

Joint Institute for Nuclear Research, Dubna

INTRODUCTION	1013
EXPERIMENT	1014
The Propane Bubble Chamber.	1014
Identification of Λ and K_s^0 .	1015
The Selection of Interactions on the Carbon Nucleus.	1017
The Measured Cross Sections of Λ and K^0 .	1019
THE Λ/π^+ RATIO FOR C + C REACTION	1020
Preview.	1020
The Λ/π^+ Ratio.	1020
THE EFFECTIVE MASS SPECTRA FOR $S = -1, -2$ MULTIBARYON STATES WITH Λ HYPERON SYSTEMS	1022
Preview.	1022
Experimental Background.	1025
(Λ, π^+) Spectra.	1025
(Λ, π^-) Spectra.	1025
(Λ, p) AND (Λ, p, p) SPECTRA	1028
The Simulated (Λ, p) Spectra in the $p + C$ Collision at 4.5 GeV/c.	1032
The Simulated (Λ, p) Spectra for the $p + D$ Collision at 30 GeV/c.	1032
(Λ, Λ) Spectra.	1032

*E-mail: paslanian@jinr.ru

(Λ , π^+ , π^-) Spectra.	1034
(Λ , p , π^-) Spectra.	1034
The Procedure of Search for $\mathbf{S} = -2 \mathbf{H}^{0+}$ Dihyperon Events.	1036
Identification of $\Xi^- \rightarrow \pi^- \Lambda$.	1039
The Background from Accidental Coincidence Events.	1040
The Observed Candidates for Light \mathbf{H}^0 and Heavy $\mathbf{H}^{0,+}$ Dihyperons.	1041
$K_s^0 p$ SPECTRA	1044
Preview.	1044
$K_s^0 p$ Spectra for All Positive Track Combinations.	1044
$K_s^0 p$ Spectra with Identified Protons.	1045
(K_s^0 , pos. tracks) Spectrum at the Momentum of $0.9 \leq p_p \leq 1.7 \text{ GeV}/c$.	1046
The Simulated $K_s^0 p$ Spectra at the Beam Momentum $4.5 \text{ GeV}/c$ for Reaction pC .	1046
$K_s^0 p$ Simulated Spectra at Beam Momentum $30 \text{ GeV}/c$ for pD Reaction.	1048
ΛK_s^0 Spectrum.	1048
$K_s^0 \pi^\pm$ SPECTRA	1048
Preview.	1048
$K_s^0 \pi^+$ Spectra.	1049
$K_s^0 \pi^-$ Spectra.	1049
CONCLUSIONS	1051
REFERENCES	1052

THE SEARCH FOR AND STUDY
OF THE STRANGE MULTIBARYON STATES
IN SYSTEMS WITH Λ HYPERON
AND K_s^0 MESON IN pA COLLISION
AT MOMENTUM OF 10 GeV/c

*P. Zh. Aslanyan**

Joint Institute for Nuclear Research, Dubna

Exotic strange multibaryon states have been observed in the effective mass spectra of $\Lambda\pi^\pm$, $\Lambda\pi^+\pi^-$, Λp , Λpp , $\Lambda\pi p$, $\Lambda\Lambda$ and ΛK_S^0 , $K_S^0 p$, $K_S^0\pi^\pm$ subsystems. The measured Λ/π^+ ratio for average multiplicities from the pC reaction is equal to $(5.3 \pm 0.8) \cdot 10^{-2}$, and it is approximately two times larger than the Λ/π^+ ratio simulated by the FRITIOF model and than that of experimental pp reactions at the same energy. The observed well-known resonances $\Sigma^{*+}(1385)$ and $K^{*\pm}(892)$ from PDG are good tests of this method. The mean value of the mass for the $\Sigma^{*-}(1385)$ resonance is shifted to 1370 MeV/c² and the width is two times larger than the same value from PDG. Such kind of behavior for the width and invariant mass of the $\Sigma^{*-}(1385)$ resonance is interpreted as an extensive contribution from stopped $\Xi^- \rightarrow \Lambda\pi^-$ and medium effect. There is enhancement of the production contribution for all observed hyperons. A few events were registered by hypothesis of light H^0 and heavy $H^{0,+}$ dihyperons. Dihyperons were observed by weak decay channels: $(\Sigma^- p)$, $(\Lambda p\pi^-)$, $(\Lambda p\pi^0)$, and $(K^- pp)$.

Измерено отношение средних множественностей Λ/π^+ для реакции pC , которое приблизительно в два раза больше, чем отношение, измеренное для реакции pC (по модели FRITIOF) и для реакции pp из эксперимента. Обнаружен ряд особенностей в спектре эффективных масс для подсистем: $\Lambda\pi^\pm$, $\Lambda\pi^+\pi^-$, Λp , Λpp , $\Lambda\pi p$, $\Lambda\Lambda$ и ΛK_S^0 , $K_S^0 p$, $K_S^0\pi^\pm$. Идентифицированы известные резонансы $\Sigma^{*\pm}(1385)$ и $K^{*\pm}(892)$ из PDG, что является хорошим тестом для этого метода. Обнаружен усиленный выход для всех зарегистрированных гиперонов. В этом эксперименте масса $\Sigma^{*-}(1385)$ резонанса смещена до значения 1370 МэВ/c², а ширина в 2 раза больше, чем значение в PDG. Такое поведение эффективной массы и ширины резонанса в $(\Lambda\pi^-)$ -спектре интерпретируется как усиленный вклад от $\Xi^- \rightarrow \Lambda\pi^-$ остановок и влияние ядерной среды. На стереофотографиях, полученных с пропановой пузырьковой камеры, обнаружены несколько событий по гипотезам легкий H^0 и тяжелый $H^{0,+}$ дигипероны со странностью $S = -2$. Дигипероны идентифицированы по каналам распада $(\Sigma^- p)$, $(\Lambda p\pi^-)$, $(\Lambda p\pi^0)$ и $K^- pp$.

PACS: 14.20.Jn; 14.40.Aq; 25.80.Nv; 25.80.Pw; 14.20.Gk; 14.40.Ev; 14.20.Pt

*E-mail: paslanian@jinr.ru

INTRODUCTION

The experimental data from the 2-m propane bubble chamber (PBC) [1–14] for events with Λ and K_s^0 particles have been analyzed to search for exotic multibaryon metastable and stable states [14–34].

There are a few topical problems of nuclear and particle physics concerning this report. These are the following goals: strange baryons in medium, the properties of cold dense baryonic matter and nonperturbative QCD [35–47], Λ yields [53–66], the confinement of quarks in hadrons, the restoration of chiral symmetry [76–232]. Strange multibaryonic clusters are an exciting possibility of exploring the properties of cold dense baryonic matter and nonperturbative QCD. Recently, the existence of discrete nuclear bound states of $\bar{K}^0 p$ has been predicted with the phenomenological Kaonic Nuclear Cluster (KNC) model which is based on the experimental information on the $\bar{K}^0 N$ scattering lengths, the kaonic hydrogen atom, and the $\Lambda^*(1405)$ resonance [35–52]. Multiquark states, glueballs and hybrids have been searched for experimentally for a very long time, but none is established.

Strange particles have been obtained extensively in hadron–nucleus and nucleus–nucleus collisions in the 4–15 GeV regions [53–58]. The experimental data from heavy ion collisions show that the K^+/π^+ ratio [64–66] is larger at BNL–AGS energies than at the highest CERN–SPS energies and even at RHIC. The experimental Λ/π^+ ratio in the pC reaction is approximately two times larger than this ratio in pp reactions or in pC reactions simulated by the FRITIOF model at the same energy [14]. However, there are no sufficient experimental data concerning strange hyperon production in hadron–nucleus and nucleus–nucleus collisions over the 4–50 GeV/ c momentum range.

A number of peculiarities were found in the effective mass spectra of $\Lambda\pi^\pm$, $\Lambda\pi^+\pi^-$, Λp , Λpp , $\Lambda p\pi$, $\Lambda\Lambda$ subsystems. The observed well-known $\Sigma^{*+}(1385)$, $\Lambda^*(1600)$, and $K^{*\pm}(892)$ resonances are good tests for this method. The width of $\Sigma^{*-}(1385)$ for the $p + A$ reaction is two times larger than that presented in PDG. The $\Lambda\pi^-$ spectra have the observed enhancement in the mass range of 1317 MeV/ c^2 which is interpreted as a stopped Ξ^- in nucleus. The cross section of stopped Ξ^- production is 4 times larger than that obtained by the FRITIOF model with the same experimental conditions. The mean value of mass for the $\Sigma^{*-}(1385)$ resonance is shifted to 1370 MeV/ c^2 and width is two times larger than the same value in PDG. Such a behavior for width and mass of the resonance in the $(\Lambda\pi^-)$ spectrum is interpreted as an extensive contribution from $\Xi^- \rightarrow \Lambda\pi^-$ stopped in medium of the nucleus. Signals for production of $\Lambda^*(1600)$, $\Lambda^*(1690)$, $\Lambda^*(1750)$, and $\Lambda^*(1850)$ resonances are observed.

At present, the existence of $S = -2$ dibaryons, which are stable against strong decays predicted by a number of theoretical models, is identified in the experiments [68–135]. A lot of efforts for H -dibaryon hunting have been made

although there have been no conclusive experimental results on the existence of the H dibaryon [136–212]. A few events, detected (Table 9) in the stereophotographs of the propane bubble chamber exposed to a 10 GeV/ c proton beam, were interpreted as $S = -2$ H^0 light ($< M_{(\Lambda\Lambda)}$) and heavy $H^{0,+}$ by weak decay channels [15–29].

Experimental efforts to find $S = +1$ Θ^+ pentaquark [16, 233] have been motivated by report [213] where antidecuplet baryons were investigated by using the chiral soliton (Skyrme) models. An opposite viewpoint is that all positive results might arise from statistical fluctuations and do not reveal a true physical effect [225].

The N^0 can be taken as a member of an antidecuplet, or an octet [213, 218] or an 27-plet [216]. On the other hand, Jaffe and Wilczek predicted a mass around 1750 MeV and a width 50% larger for these states than those of the Θ^+ [215]. These peaks could be interpreted as possible candidates for two pentaquark states [20, 21]: the N^0 with the quark content $udsds$ decaying into ΛK_s^0 and the Ξ^0 resonance with the quark content $udssd$ decaying into $\Lambda \bar{K}_s^0$.

The scalar mesons have vacuum quantum numbers and are crucial for the full understanding of the symmetry breaking mechanisms in QCD, and presumably also for confinement. In the recent topical review [232] it was suggested that the lightest scalars are at the central core composed of four quarks. There are theoretical arguments in favor of a light and broad $\kappa(800)$ [231] pole near the $K\pi$ threshold. However, the experimental evidence is not conclusive [22–30, 239–243].

A survey of new experiments with much improved statistics compared to those early PBC data would hopefully answer the question whether such «exotic» multi-quark hadron and baryon resonances exist.

1. EXPERIMENT

1.1. The Propane Bubble Chamber. Reliable identification of the above-mentioned resonances requires to use 4π detectors and high-precision measurements of the sought objects. The full experimental information of more than 700 000 stereophotographs or 10^6 p +propane inelastic interactions from the 2-m propane bubble chamber at JINR, LHE, at 10 GeV/ c are used to select events with strange particles V^0 [1–15]. The conditions for primary proton beams are $\tan \alpha < 0.02$, $1.62 < \beta < 1.69$ rad. The effective ranges for registration of stars by the Y coordinate are $-80 \leq Y_I \leq -20$ cm and $10 \leq Y_{II} \leq 80$ cm for the first and second parts of the chamber, respectively. The fit of the GRIND-based program GEOFIT [2, 3] is used to measure the kinematic parameters of the tracks: p , α , and β . Measurements were repeated three times for all events and fit by GEOFIT. The momentum resolution of charged particles

is $\langle \Delta P/P \rangle = 2.1\%$ for stopped particles and $\langle \Delta P/P \rangle = 9.8\%$ for nonstopped particles. The mean values for the errors of the dip and azimuthal angles are equal to $\langle \Delta \tan \alpha \rangle = (0.0099 \pm 0.0002)$ and $\langle \Delta \beta \rangle = (0.0052 \pm 0.0001)$ rad.

The estimation of ionization for charged tracks and length for stopped particles permitted one to identify them over the following momentum ranges [15]: protons of $0.150 < P_p < 0.900$ GeV/c and K^\pm of $0.05 < P_p < 0.6$ GeV/c.

1.2. Identification of Λ and K_s^0 . The events with V^0 (Λ and K_s^0) were identified by using the following criteria [5–15]: 1) V^0 stars from the photographs were selected according to the $\Lambda \rightarrow \pi^- + p$, $K_s^0 \rightarrow \pi^- + \pi^+$, and $\gamma \rightarrow e^+ + e^-$ hypotheses. The low-momentum limits of K_s^0 and Λ are greater than 0.1 and 0.2 GeV/c, respectively; 2) V^0 stars should have the effective masses of K_s^0 and Λ ; 3) the V^0 momentum and the momenta of the particles from the V^0 decay are located in the same plane (coplanarity); 4) they should have one-vertex–three-constraint (1V3C) fit for the M_K or M_Λ hypothesis and after the fit, $\chi_{V^0}^2$ should be selected over the range smaller than 12; 5) the analysis of the experimental data has shown that the events with undivided ΛK_s^0 were assumed to be Λ hyperons [5, 14].

All V^0 are classified into three groups. The first group comprises V^0 s events which could be uniquely identified with the above criteria (1–4) and with bubble densities from the positive track of V^0 s, too. The second grade comprises V^0 s, which could be undivided ΛK_s^0 . For correct identification of the undivided V^0 s, the α (Armenteros parameter) and the $\cos \theta_{\pi^-}^*$ distributions (Fig. 1) are used

$$\alpha = (P_{\parallel}^+ - P_{\parallel}^-)/(P_{\parallel}^+ + P_{\parallel}^-), \quad (1)$$

where P_{\parallel}^+ and P_{\parallel}^- are the momentum components of positive and negative charged tracks relative to the direction of the V^0 momentum; $\theta_{\pi^-}^*$ is the angle between π^- (from V^0 decay) and V^0 in the V^0 rest frame. α (Fig. 1) and the $\cos \theta_{\pi^-}^*$ distributions from the $K_s^0(\Lambda)$ decay were isotropic in the K_s^0 rest frame after removal of undivided $K_s^0(\Lambda)$. Then these $K_s^0(\Lambda)$ events were assumed to be Λ hyperons. After this, we show in Fig. 1, *c* that the $\cos \theta_{\pi^-}^*$ distributions for the $\Lambda + K_s^0(\Lambda)$ s are also isotropic in the V^0 rest frame. The results of the above procedure are as follows: the loss of K_s^0 is 8.5% and the admixture of K_s^0 in Λ s events is 4.6%. The third group comprises V^0 s which could be invisible V^0 s at a large azimuth angle ϕ [5]. The average ϕ weights are equal to $\langle w_\phi \rangle = 1.06 \pm 0.02$ for K_s^0 and $\langle w_\phi \rangle = 1.14 \pm 0.02$ for Λ .

Figures 2, *a*, *c* and *b*, *d* show the effective mass distribution of Λ (8657 events), K_s^0 (4122 events) particles and their χ^2 from kinematics fits, respectively. The expected functional form for χ^2 is depicted by the dotted histogram. Each V^0 event has a weight w_{geom} , where the average geometrical weights are 1.34 ± 0.03 for Λ and 1.22 ± 0.04 for K^0 [15].

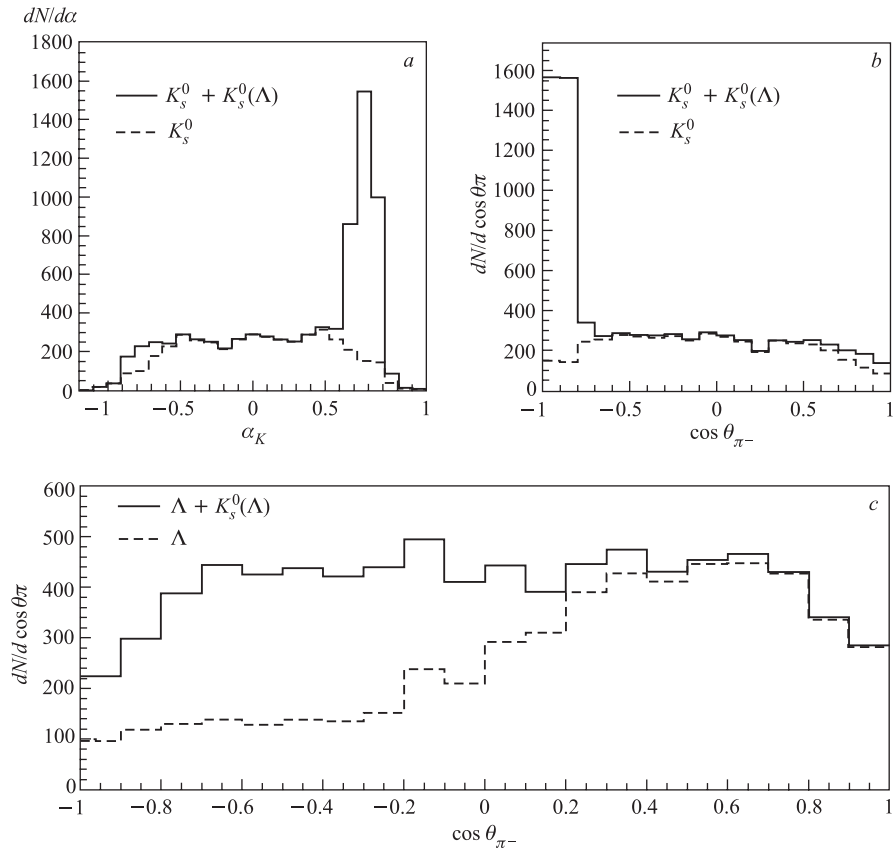


Fig. 1. Distributions of α (Armenteros parameter) and $\cos \theta^*$ used for correct identification of the undivided $K_s^0(\Lambda)$. $\alpha = (P_{\parallel}^+ - P_{\parallel}^-)/(P_{\parallel}^+ + P_{\parallel}^-)$, where P_{\parallel}^+ and P_{\parallel}^- are the parallel components of momenta of positive and negative charged tracks from the V^0 relative to the direction of the V^0 momentum. $\cos \theta^*$ is the angular distribution of π^- from $K_s^0(\Lambda)$ decay in the rest frame of $K_s^0(\Lambda)$. Distributions of α and $\cos \theta$ must be isotropic in the rest frame of K_s^0 . Therefore, undivided ΛK_s^0 must be assumed as Λ hyperons

A possibility of imitating Λ and K_s^0 by neutron stars was made by the FRITIOF model [12]. The hypothesis reactions $p + \text{propane} \rightarrow n + X$, $n + \text{propane} \rightarrow \pi^- p$ (or $\pi^- \pi^+$) X^0 with Fermi motion in carbon were simulated. Then, these events were analyzed by using the same experimental conditions as those used for the selection of V^0 s. This analysis showed that the background from neutron stars was $\leq 0.1\%$ for Λ and $\leq 0.001\%$ for K_s^0 events.

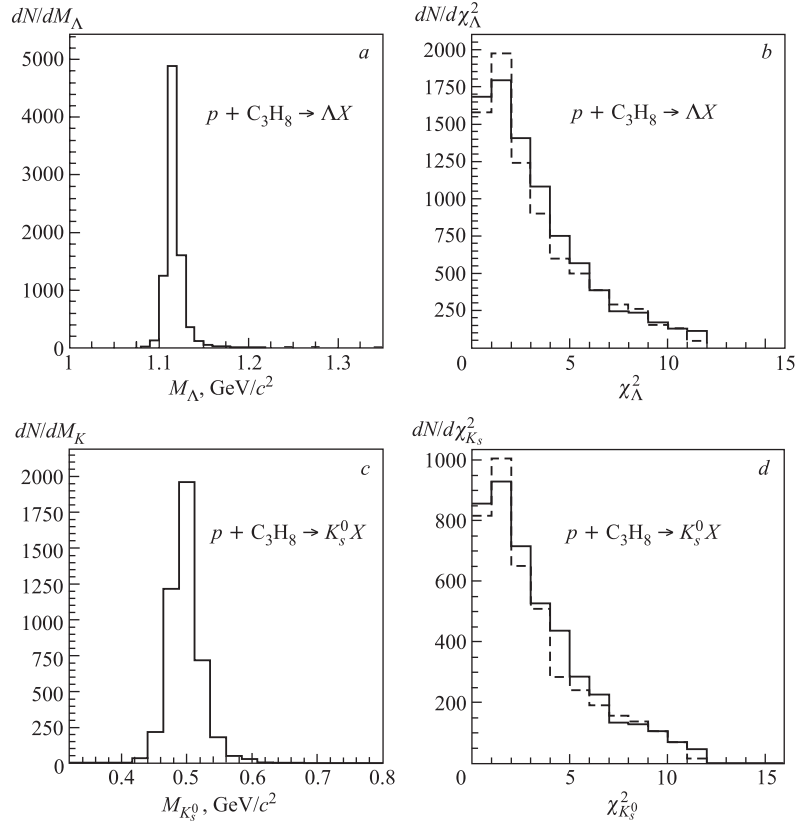


Fig. 2. Distribution of experimental V^0 events from interactions of beam protons with propane: a) for the effective mass of M_Λ ; b) for $\chi_\Lambda^2(1V - 3C)$ of the fits via the decay mode $\Lambda \rightarrow \pi^- + p$; c) for the effective mass of $M_{K_s^0}$; d) for $\chi_{K_s^0}^2(1V - 3C)$ of the fits via decay mode $K_s^0 \rightarrow \pi^- + \pi^+$. The expected functional form of χ^2 is depicted by the dotted histogram

1.3. The Selection of Interactions on the Carbon Nucleus. The $p + C \rightarrow \Lambda(K_s^0)X$ reactions were selected from C_3H_8 by using the following criteria [4,7]:

1. $Q = n_+ - n_- > 2$;
2. $n_p + n_\Lambda > 1$;
3. $n_p^b + n_\Lambda^b > 0$;
4. $n_- > 2$;
5. $n_\pm = 2k + 1$ ($k = 0, 1, 2$);
6. $m_t = (E_p(\Lambda) - P_{p(\Lambda)} \cos(\Theta_{p(\Lambda)})) > m_p$.

n_+ and n_- are the number of positive and negative particles on the star; n_p and n_Λ are the number of protons and Λ hyperons with the momentum $P < 0.75$ GeV/c on the star; n_p^b and n_Λ^b are the number of protons and Λ hyperons emitted in the backward hemisphere; $E_{p(\Lambda)}$, $P_{p(\Lambda)}$, and $\Theta_{p(\Lambda)}$ are the energy, momentum, and emission angle of protons (or Λ s) in the lab. system; m_t and m_p are the effective target mass and the proton mass, respectively. Only $\approx 83\%$ inelastic $p + C$ interactions were separated by these criteria [8].

The $p + \text{propane} \rightarrow \Lambda(K_s^0)$ reaction was simulated by using the FRITIOF model [12] with experimental conditions. Then the influence of above criteria was analyzed when pC interactions were selected from the simulated $p + \text{propane} \rightarrow \Lambda(K_s^0)$ reactions. This simulation showed that the lost events were 18 and 20% from the interactions $pC \rightarrow \Lambda X$ and $pC \rightarrow K_s^0 X$, respectively. These results

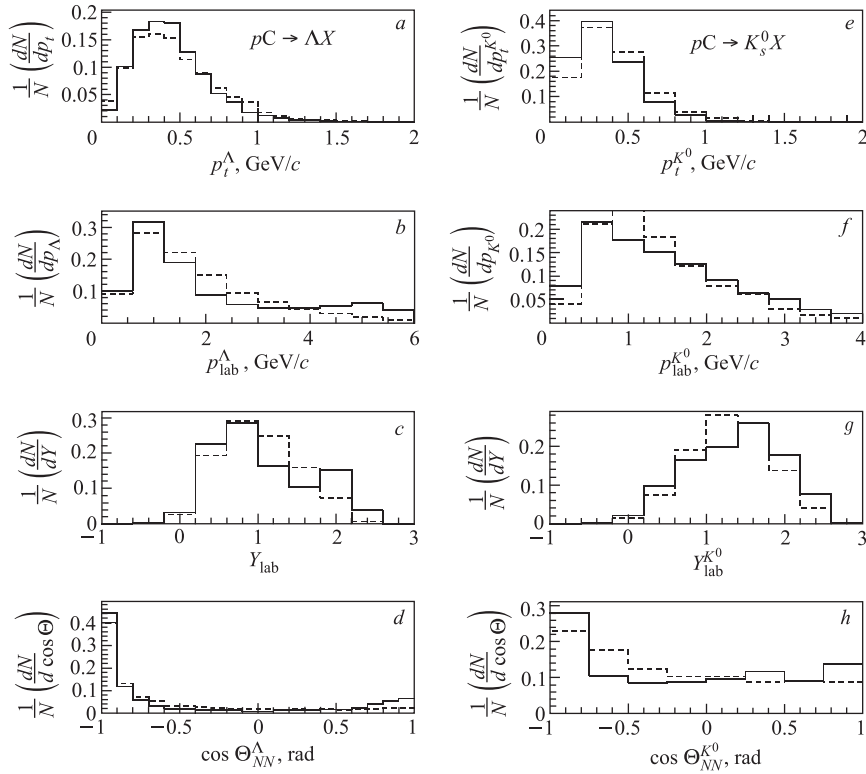


Fig. 3. Experimental (dashed) and FRITIOF-simulated (solid) distributions of Λ hyperons and K_s^0 mesons in the $p + C$ interaction at 10 GeV/c: *a, e*) in the transverse momentum p_t , GeV/c; *b, f*) in the momentum p_{lab} , GeV/c; *c, g*) in the longitudinal rapidity Y_{lab} ; *d, h*) in the azimuthal angle $\cos \Theta$ (in the CM of $p + p$ collisions)

are obtained without correcting by condition, when all undivided $K_s^0(\Lambda)$ were assumed to be Λ hyperons. Contributions from the reactions $pp \rightarrow \Lambda X$ and $pp \rightarrow K_s^0 X$ in reactions of $pC \rightarrow \Lambda X$ and $pC \rightarrow K_s^0 X$ were estimated by the FRITIOF model similarly and they were 1.0 and 0.3%, respectively.

Figure 3 compares the momentum, $\cos \theta$ in the c.m. nucleon–nucleon system, transverse momentum p_t , and longitudinal rapidity distributions of Λ and K_s^0 for experimental events (dashed line) and those simulated by the FRITIOF model (solid line) in $p+C$ interactions, which are selected from $p+\text{propane} \rightarrow \Lambda(K_s^0)X$. From Fig.3 one can see that the experiment is described by the FRITIOF model satisfactorily.

1.4. The Measured Cross Sections of Λ and K^0 . The cross section is defined by the formula:

$$\sigma = \frac{\sigma_0 N_r^{V^0}}{e} \prod_i w_i = \frac{\sigma_r N_r^{V^0} w_{\text{hyp}} w_{\text{geom}} w_\phi w_{\text{kin}} w_{\text{int}}}{N_r e_1 e_2 e_3}, \quad (2)$$

where $1/e_1 = 1.14 \pm 0.04$ is the efficiency of the search for V^0 in the photographs, $1/e_2 = 1.25 \pm 0.02$ is the efficiency of measurements and collection of V^0 events after all measurements, e_3 is the probability of decay via the channel of charged particles ($\Lambda \rightarrow p\pi^-, K^0 \rightarrow \pi^+\pi^-$), $\sigma_0 = \sigma_r/N_r$ is the total cross section, where σ_r is the total cross section for registered events, $N_r^{V^0}$ and N_r (≈ 750000) are the experimental number of registered V^0 s and $p+C$ interactions over the effective range of the chamber, respectively; $\sigma_t(p+C_3H_8) = 3\sigma_{pC} + 8\sigma_{pp} = (1456 \pm 88)$ mb [13], where σ_t, σ_{pC} , and σ_{pp} are the total cross sections in interactions of $p+C_3H_8, p+C$, and $p+p$, respectively. The propane bubble chamber method permitted the registration of the part of all elastic interactions with the propane; therefore, the total cross section of the registered events is $\sigma_r(p+C_3H_8) = 3\sigma_{pC}(\text{inelastic}) + 8\sigma_{pp}(\text{inelastic}) + 8\sigma_{pp}(\text{elastic}) 0.70 = (1049 \pm 60)$ mb [6, 7].

Registration efficiencies obtained for experimental conditions are defined as $e_i = n_i/N$ and $\Delta e_i = \sqrt{e_i(1+e_i)/N}$, where n is the number of selected events with some experimental conditions and N is the total number of events.

The experimental cross sections for the interactions $pp \rightarrow \Lambda X$ and $pp \rightarrow K_s^0 X$ at the beam momentum 10 GeV/c are taken from the compilation for cross sections and they are (0.8 ± 0.08) mb for Λ hyperons and (0.43 ± 0.04) mb for

Table 1. Cross sections for production of Λ hyperons and K_s^0 mesons in the pC interaction at the beam momentum 10 GeV/c

Type of reaction	$N_{V^0}^{\text{exp.}}$	$W_{\text{sum}} = \prod_i w_i$	$N_{V^0}^{\text{total}}$	$n_{V^0} = N_{V^0}^t/N_{\text{in}}$	σ , mb
$pC \rightarrow \Lambda X$	6126	4.37	26770	0.053	13.3 ± 1.7
$pC \rightarrow K_s^0 X$	3188	2.93	9341	0.018	4.6 ± 0.6

K_s^0 mesons. The experimental inclusive cross sections for Λ and K_s^0 production in the $p^{12}\text{C}$ collision are equal to $\sigma_\Lambda = (13.3 \pm 1.7)$ and $\sigma_{K_s^0} = (4.6 \pm 0.6)$ mb, respectively [14] (Table 1).

2. THE Λ/π^+ RATIO FOR C + C REACTION

2.1. Preview. Strange particles have been extensively obtained in hadron–nucleus and nucleus–nucleus collisions at 4–15 GeV [53–58]. The number of Λ s produced in the $\bar{p} + \text{Ta}$ reaction at 4 GeV/c was 11.3 times larger than that expected from the geometrical cross section in the KEK 1-m hydrogen bubble chamber [53]. In experiments AGS with Au(Si) + Au collisions at 10.7 [56], 11.6 [57], and 14.6A GeV/c [58], the $K^+/\pi^+(\Lambda/\pi^+)$ ratio is four-to-five times larger than the $K^+/\pi^+(\Lambda/\pi^+)$ ratio from the $p+p$ reaction at the same energy. In heavy ion Pb + Pb central interactions (NA49 Collaboration) the K^+ yield from $p+p$ reactions increases faster with increasing beam energy as compared with the π^+ yield (K^+/π^+ ratio) from $p+p$ reactions at momenta 4–160A GeV/c [64–66] (Fig. 4, a). Therefore, the analysis of strange hyperon and K^+ total yields [64–66] is of great interest as an indicator of strange quark production. If the hadronic rescattering mechanism dominates strangeness enhancement at 10A GeV, how rapidly does it reduce as the beam energy increases [65]? This behavior is of particular interest as it could be a signal of new dynamics for strangeness production. Strangeness enhancement was analyzed regarding such reaction mechanisms as a possible signature for the quark–gluon plasma(QGP) [59,60], as the multinucleon effect [61], or the fireball effect [62], or as the deconfiment signal, within the context of thermal equilibration models [63–66].

It has already been experimentally observed in the energy dependence of the K^+/π^+ ratio and is predicted to be even more pronounced in the Λ/π^+ ratio [63–66].

2.2. The Λ/π^+ Ratio. Ratios of average multiplicities of Λ hyperons and K_s^0 mesons to multiplicities of π^+ mesons in the $p + \text{C}$ interaction at beam momenta 4.2 and 10 GeV/c are shown in Table 2. The experimental Λ/π^+ ratio agrees with the FRITIOF simulated ratio at the momentum 4.2 GeV/c (Table 2), but at the momentum 10 GeV/c it is approximately two times larger than the FRITIOF ratio in the reaction $p\text{C}$.

The Λ/π^+ ratio for the C + C reaction is shown in Table 3 and in Fig. 4, b. This Λ/π^+ ratio for the C + C reaction at the momentum 10 GeV/c was obtained by using the FRITIOF model and the Glauber approach from the experimental cross section for the $p + \text{C} \rightarrow \Lambda X$ reaction. As can be seen from the experimental data in Table 3 and the thermal statistical model (Fig. 4, b) there is pronounced enhancement especially for the Λ/π^+ ratio at 10–15A GeV/c.

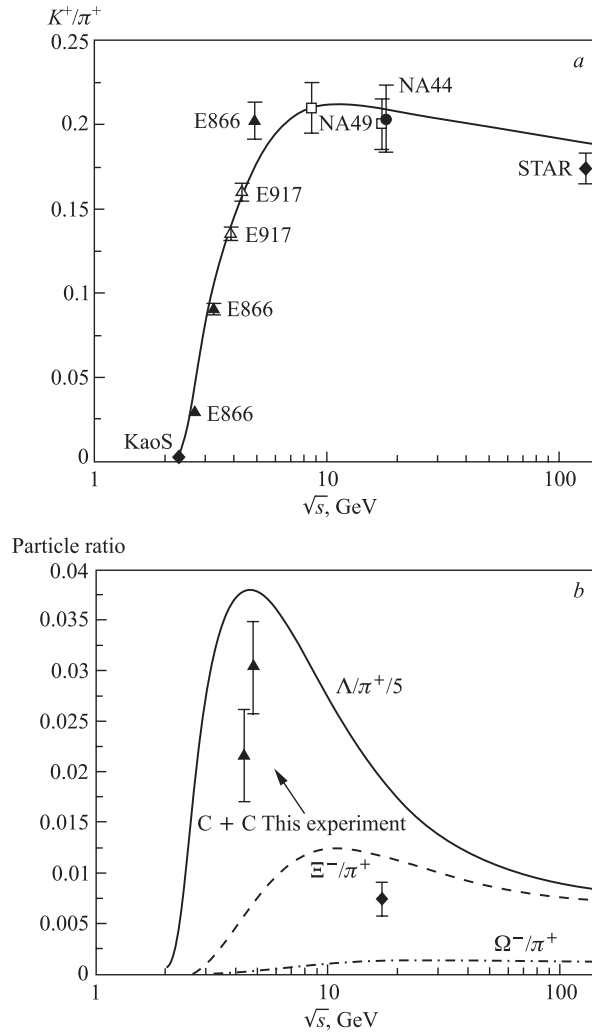


Fig. 4. *a)* K^+/π^+ ratio obtained around midrapidity as a function of \sqrt{s} from the various experiments. For the references for all data points see [63,64]. The solid line shows the results of the statistical model in complete equilibrium. The value at RHIC was estimated using the results from the STAR Collaboration on the K^-/π^- and K^+/K^- ratios, assuming $\pi^-/\pi^+ = 1.007$. *b)* The prediction of the statistical-thermal model [64] for Λ/π^+ (solid line, note that this ratio is divided by 5), and Ξ^-/π^+ (dashed line) and Ω^-/π^+ (dash-dotted line) ratios as a function of \sqrt{s} . For compilation of AGS data see [66]. The Λ/π^+ ratio in the interaction C + C in the figure is obtained by using the data from this experiment

Table 2. Ratios of average multiplicities of Λ hyperons and K_s^0 mesons to multiplicities of π^+ mesons for the $p + C$ interaction at beam momenta 4.2 and 10 GeV/c

Ratios, 10^2	pC (this experiment, 10 GeV/c)	pC (FRITIOF, 10 GeV/c)	Cp (experiment [4], 4.2 GeV/c)	Cp (FRITIOF, 4.2 GeV/c)
(n_Λ/n_{π^+})	5.3 ± 0.8	2.6	0.7 ± 0.3	0.9
$(n_{K_s^0}/n_{\pi^+})$	1.8 ± 0.3	1.8	0.3 ± 0.2	0.3

Table 3. Ratios of average multiplicities of Λ hyperons to multiplicities of π^+ mesons for $C + C$ interaction at the beam momentum 4.2 and 10 GeV/c

Ratios, 10^2	4.2 GeV/c [4, 8], experiment	10 GeV/c, experiment
(n_Λ/n_{π^+})	2.0 ± 0.6	10.9 ± 1.7

3. THE EFFECTIVE MASS SPECTRA FOR $S = -1, -2$ MULTIBARYON STATES WITH Λ HYPERON SYSTEMS

3.1. Preview. The first evidence for Quantum Chromodynamics (QCD), the theory of the strong interactions, came from the systematics of baryon and meson spectroscopy. As far back as 1977, Jaffe [68], using the bag model in which confined colored quarks and gluons interact as in perturbative QCD, suggested the existence of a light nonet composed of four-quark mesons, five-quark baryons, six-quark dibaryons, etc. Multiquark resonance formation with Λ hyperons via the compression mechanism reduces to the phase transition of normal density to superstrange hadronic matter revealing itself as multibaryon resonances in the above presented models and especially in the bag models calculation in [68, 69, 134, 135].

The H dibaryon is a spin and isospin singlet, spin-flavor symmetric, positive parity state composed of six quarks ($uuddss$). Many theoretical calculations of the H -dibaryon mass and structure were performed using various models and theories [68–135]. Since Jaffe's prediction, many theoretical calculations were made to predict the mass of the H dibaryon, employing various QCD-inspired models: bag model [69–80], nonrelativistic quark cluster model [88, 89–98], Skyrme model [81–87], and so on [107–118], QCD sum rule [102, 103] and lattice QCD [99–101]. Many of them predict the bound state. However, the results of calculations spread over a wide range as shown in Fig. 16. Theoretical analyses of the production [119, 189–203] of the H dibaryon in various processes were performed mainly by the coalescence model.

The H dibaryon may exist in another environment, e.g., in a double hypernucleus or in some special astrophysical objects. Double hypernucleus data

have important meaning for the existence of the H dibaryon in the sense that the binding energy of two Λ s is related to the lower limit of the H -dibaryon mass. However, whether the $S = -2$ component in a double hypernucleus takes the form of $\Lambda\Lambda$ is not a trivial problem, and it is possible that a double hypernucleus is an H -nucleus state [207,212]. The possibility that H -dibaryon matter may exist in the core of a neutron star was also pointed out [211]. Consider a double hypernucleus which is formed by the fusion of a nonstrange nucleus and two Λ s with their binding energy $B_{\Lambda\Lambda} = M(^{A-2}Z) + 2M_{\Lambda} - M(^{A}_{\Lambda\Lambda}Z)$. Therefore, the existence of a double hypernucleus means that the mass of the H dibaryon should be heavier than the mass of the two Λ s minus the binding energy: $M_H > 2M_{\Lambda} - B_{\Lambda\Lambda}$. A few events of double hypernuclei were reported. Old nuclear emulsion experiments reported $^{10}_{\Lambda\Lambda}\text{Be}$ [204] and $^{6}_{\Lambda\Lambda}\text{He}$ [205]. The former was reanalyzed by Dalitz et al. [208]. An emulsion-counter hybrid experiment (KEK E176) reported that an event [206] can be interpreted as $^{10}_{\Lambda\Lambda}\text{Be}$ [206,209] or $^{13}_{\Lambda\Lambda}\text{B}$ [206,209,210]. Many projects for double hypernucleus hunting are going on. The estimated binding energy of the H particle is model-dependent, and ranges from positive (unbound) to -650 MeV (quite strongly bound).

A single mass formula inspired by the spinflavour $SU(6)$ -symmetry breaking is used to estimate the hyperon binding energies of Λ , double Λ , Σ , cascade and θ hypernuclei [47]. The Λd and Σd scattering lengths were obtained by using baryon-baryon interactions from a chiral constituent quark model, which correctly predicts the hypertriton binding energy [46].

Instead of the Yukawa mechanism for intermediate-range attraction, some new approaches, based on formation of the symmetric six-quark bag in the state $|(0_s)6[6]x, L = 0\rangle$ dressed due to strong coupling to π , σ , and ρ fields, are suggested [71].

Recently, exotic light nuclear systems involving \bar{K} (K^- and \bar{K}^0) as a constituent have been predicted on the basis of phenomenologically constructed $\bar{K}N$ interactions [35–39]. One of the most obvious candidates for the simplest KNC can be the strange baryon $\Lambda(1405)$ with the mass $m_{\Lambda(1405)} = (1406 \pm 4)$ MeV and the width $\Gamma_{\Lambda(1405)} = (50 \pm 2)$ MeV [10]. According to Akaishi and Yamazaki [35], the strange baryon $\Lambda(1405)$ can be treated as a bound K^-p pair or $\frac{K}{1}H$ with isospin $I = 0$. The exotic structure involving a K was also studied by the Antisymmetrized Molecular Dynamics method by Dote et al. [39]. This method can predict the density distributions of the constituent \bar{K} , protons, and neutrons, as shown in Fig. 5.

The FINUDA (INFN), FOPI (GSI), OBELIX (CERN), PS E549 (KEK) and PS E471 (KEK) Collaborations also reported [43–52] results of the analysis of the Λp and Λd correlations (Table 4).

At present the experimental situation is confusing; so is theory. No exotic mesons and exotic baryons (except for recent discoveries) have been observed either. The classic example is a baryon with positive strangeness, a Z as it is

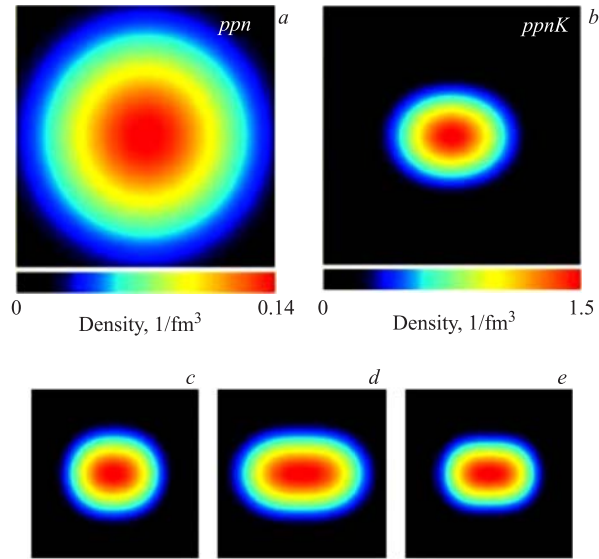


Fig. 5. Calculated density contours of $ppnK^-$. Comparison between usual ${}^3\text{He}$ (a) and ${}^3\text{He}K^-$ (b). Individual contributions of the proton (c), neutron (d) and K^- (e) are given in the size of 3 by 3 fm

Table 4. Effective mass, width (Γ) and S.D. for observed exotic strange resonances

Collaboration	Type of collisions	Resonance decay mode	$M_{\text{res}}, \text{MeV}/c^2$	$\Gamma \approx, \text{MeV}/c^2$	Statistical significance S.D.
FOPI	Al + AL	Λp	2120 ± 10	59 ± 12	5.0
	Ni + Ni		2140 ± 10	59 ± 19	5.4
FINUDA	K^- stopped in ${}^{12}\text{C}$ and ${}^{6,7}\text{Li}$	Λp	2255 ± 9	67 ± 14	7(10)
Obelix	p stopped ${}^4\text{He}$	Λp	2209	< 24.4	3.7
FOPI	Ni + Ni	Λd	3149 ± 15	100 ± 49	4.9
FINUDA	K^- stopped in ${}^6\text{Li}$	Λd	3251 ± 6	37 ± 14	3.9
KEK549	K^- stopped in He	Λd	—	—	—
Obelix	\bar{p} stopped in ${}^4\text{He}$	Λd	3190 ± 15	< 60	2.6

known, with the valence quark content $uud\bar{s}$ [67]. Despite years of theoretical and experimental work, QCD has not yet yielded the secrets of confinement dynamics, the structure of quark correlations and the problem of exotics. These are fundamental questions of great importance in particle physics.

3.2. Experimental Background. The total experimental background has been obtained by three methods. The first is a polynomial method, where the experimental distribution on effective mass with removed areas of the resonance was approximated by the polynomial function, while this procedure provided the fit with $\chi^2 \approx 1$ and the polynomial coefficient with errors of less than 30%.

The second is a mixing method, where the angle between decaying particles for experimental events is randomly mixed (described in [11]). This background was obtained using our experimental condition. Then, the effective mass distribution was fitted by the polynomial function.

The third type of background for the effective mass was obtained by the FRITIOF model [12]. In all figures, the simulated background distribution was normalized to the experimental distribution.

The signal from the resonance is identified by using the fit with formula [9]

$$\frac{d\sigma(M)}{dm} = \text{BG}(M) + \text{BW}(M) \cdot \text{PS}(M),$$

where BG is the background, BW is the Breit–Wigner function, and PS is phase space.

The statistical significance of resonance peaks was calculated as $\text{NP}/\sqrt{\text{NB}}$, where NB is the number of counts in the background under the peak, and NP is the number of counts in the peak above the background.

3.3. (Λ, π^+) Spectra. The $\Lambda\pi^+$ effective mass distribution for all 19534 combinations with the bin size $12 \text{ MeV}/c^2$ is shown in Fig. 6, *a* [27–30]. The bin size is consistent with the experimental resolution. The upper dashed curve (Fig. 6, *a*) is the sum of the background and 1 Breit–Wigner function ($\chi^2/\text{n.d.f.} = 79/95$). The background (lower dashed curve) is the six-order polynomial function (Fig. 6, *a*). The dashed histogram is always the simulated background by the FRITIOF model in the figures. The mass resolution is $\Delta M/M = 0.7\%$ in the mass range of $\Sigma^{*+}(1382)$. The decay width is $\Gamma \approx 45 \text{ MeV}/c^2$. The cross section of $\Sigma^{*+}(1382)$ production (≈ 540 exp. events) is approximately 0.9 mb for the $p + \text{C}$ interaction. This observed resonance $\Sigma^{*+}(1382) \rightarrow \Lambda\pi^+$ was a good test of this method.

Figure 6, *b* shows the $\Lambda\pi^+$ spectrum in the momentum range $P_p < 1 \text{ GeV}/c$ with the bin size $14 \text{ MeV}/c^2$ for 9095 combinations, where combinations with protons are removed. In Fig. 6, *b*, the $\Lambda\pi^+$ spectrum (dashed curve) is approximation by the eight-order polynomial form with $\chi^2/\text{n.d.f.} = 459/98$. In this case, the $\Lambda\pi^+$ spectrum is described by the FRITIOF model satisfactorily (Fig. 6, *b*).

3.4. (Λ, π^-) Spectra. The $\Lambda\pi^-$ -effective mass distribution for all 6465 combinations with the bin sizes of 14 and $8 \text{ MeV}/c^2$ are shown in Fig. 6, *c, d*. The upper dashed curve (Fig. 6, *c*) is the sum of the background (by the eight-order polynomial) and 1 BW function ($\chi^2/\text{n.d.f.} = 41/54$). There is significant enhancement in the mass range of $1370 \text{ MeV}/c^2$, with 12.5 S.D., $\Gamma = 92 \text{ MeV}/c^2$.

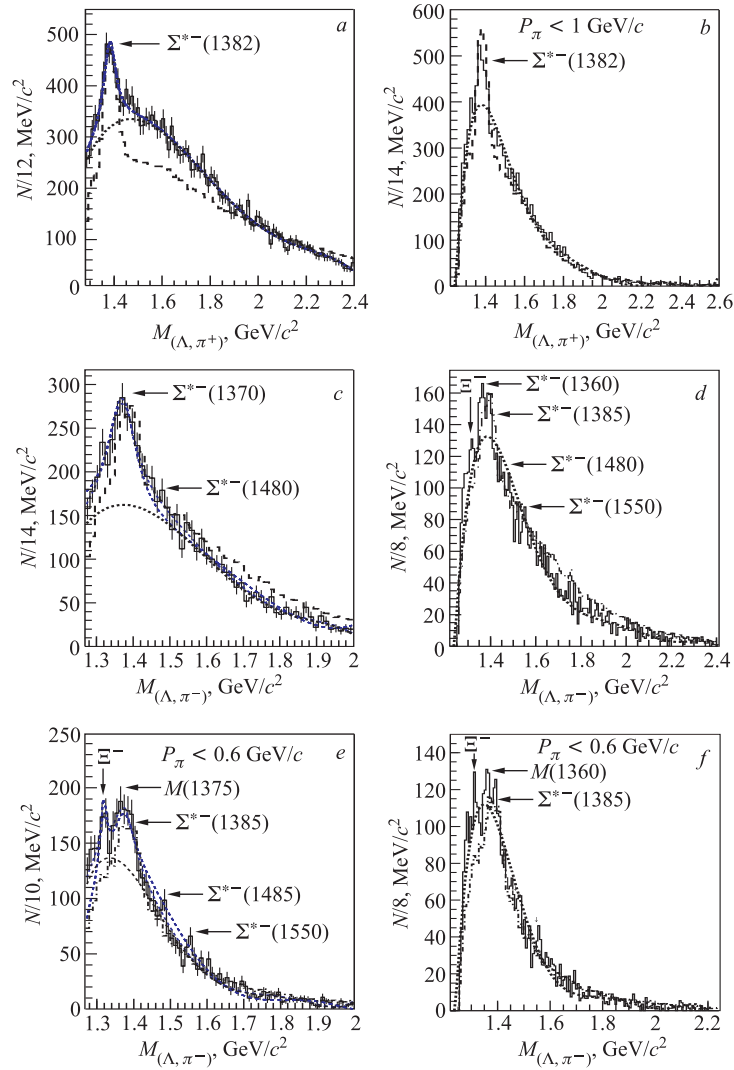


Fig. 6. *a*) The $\Lambda\pi^+$ spectrum for all combinations with the bin size of $12 \text{ MeV}/c^2$; *b*) $\Lambda\pi^+$ spectrum in the momentum range of $P_\pi < 1 \text{ GeV}/c$ with the bin size of $14 \text{ MeV}/c^2$; *c*) $\Lambda\pi^-$ spectrum for all combinations with the bin size of $14 \text{ MeV}/c^2$; *d*) $\Lambda\pi^-$ spectrum for all combinations with the bin size of $8 \text{ MeV}/c^2$; *e*) $\Lambda\pi^-$ spectrum in the momentum range of $P_\pi < 0.6 \text{ GeV}/c$ with the bin size of $10 \text{ MeV}/c^2$; *f*) $\Lambda\pi^-$ spectrum in the momentum range of $P_\pi < 0.6 \text{ GeV}/c$ with the bin size of $8 \text{ MeV}/c^2$. The events simulated by FRITIOF model are shown by the dashed histogram. The background is shown by the dashed curve

The cross section of Σ^{*-} production (≈ 680 events) is ≈ 1.3 mb at 10 GeV/c for the $p + C$ interaction. The observed width for Σ^{*-} is ≈ 2 times larger than the PDG value. One of the possible explanations is nuclear medium effects on invariant mass spectra of hadrons decaying in nuclei [42]. There is also significant enhancement in the mass range of 1480 MeV/c² (3.9 S.D.). There are small enhancements in the mass ranges of 1320, 1520, and 1550 MeV/c². Figure 6, *d* shows the same effective mass distribution with the bin size of 8 MeV/c², where there are enhancements in the same mass regions of 1320, 1480, 1520, and 1550 MeV/c², too. In this case, the peak in the mass range of $M(1370)$ decays into three ranges: $M(1317)+M(1360)+M(1385)$, where $M(1317)$ and $M(1385)$

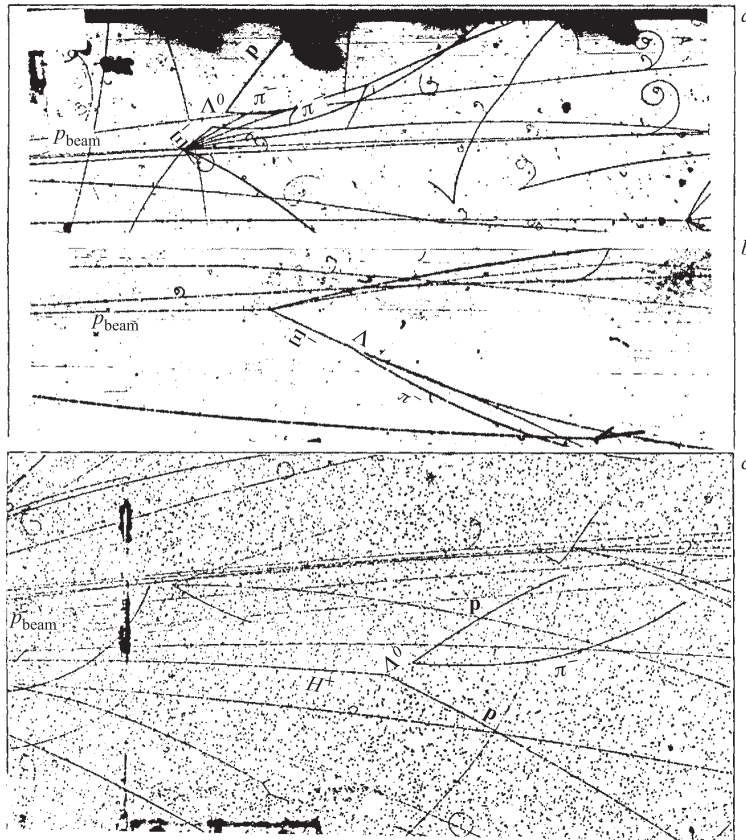


Fig. 7. *a, b*) The candidates for the Ξ^- hyperon were observed in the sample of the so-called one-negative-prong secondary events imitating a weak decay $\Xi^- \rightarrow \Lambda + \pi^-$. *c*) The candidate H^+ dihyperon was observed in the sample of the so-called one-positive-prong secondary event which imitates the weak decay $H^+ \rightarrow p + \Lambda^0 + \gamma$ or $p + \Lambda + \pi^0$ [15]

can be interpreted as contributions from Ξ^- and $\Sigma^{*-}(1385)$. Then the $M(1360)$ peak can be interpreted as contribution from phase space or medium effect with $\Sigma^{*-}(1385)$ in the carbon nucleus.

Figure 6, *e, f* shows the $\Lambda\pi^-$ effective mass distribution for 3829 combinations with the bin sizes 10 and 8 MeV/ c^2 over the momentum range of $P_\pi < 0.6$ GeV/ c , where combinations with K^- are removed. The upper dashed curve (Fig. 6, *e*) is the sum of the background (eight-order polynomial) and 2 BW function ($\chi^2/\text{n.d.f.} = 81/73$). After the fit of this effective mass distribution by 2 BW function, the observed width for $\Sigma^{*-}(1375)$ is ≈ 58 . In this case the width decreased and is ≈ 1.5 times larger than the PDG value.

Figure 6, *f* shows that the spectrum in the mass range of $M(1375)$ decays into two mass ranges $M(1360) + M(1385)$. After the cut of $P_p < 0.6$ GeV/ c the behavior of the $\Lambda\pi^-$ spectrum is not changed. The dashed curve (Fig. 6, *f*) is a six-order polynomial. There are small enhancements in the mass regions of 1320 (4.1 S.D.), 1480 (4.2 S.D.), and 1550 (3.7 S.D.) MeV/ c^2 . The number of Ξ^- stopped in nuclear medium is ≈ 60 events for $p + \text{propane}$ interaction. The observed experimental cross section for stopped Ξ^- is more than 4 times larger than the cross section which is obtained by the FRITIOF model for the same experimental conditions. The total number of events w by the weak decay channel with Ξ^- is ≈ 16 (where $w = 1/e_\Lambda = 5.3$ is a full geometrical weight of registered Λ s) [15]. Then the experimental cross section for identified Ξ^- by weak decay channel [15] (Fig. 7) is more than two times larger than that from the calculation by FRITIOF. In this bin case, the width of $\Sigma^{*-}(1375)$ for the $p + A$ reaction is ≈ 1.5 times larger than that presented in the PDG.

Figure 7 shows that there is a significant enhancement in the mass ranges of $\Sigma^{*-}(1480)$ which agrees with the report from the SVD2 Collaboration, too [237].

4. (Λ, p) AND (Λ, p, p) SPECTRA

Figure 8, *a* shows the invariant mass for all Λp 21500 combinations with the bin size of 8 MeV/ c^2 [24]. There are small enhancements in the mass regions of 2100, 2212, and 2310 MeV/ c^2 (Fig. 8, *a*). There is a significant signal in the region of 2155 MeV/ c^2 (≥ 6 S.D.)

There are published reports [24–29] for the (Λp) invariant mass with identified protons in the momentum range of $0.350 < P_p < 0.900$ GeV/ c (Fig. 8, *b*). The solid curve is the sum of the background obtained by the polynomial method and 4 Breit–Wigner resonance (BW) curves (Fig. 8, *b*). There are significant enhancements in the mass regions of 2100, 2175, 2285, and 2353 MeV/ c^2 . Their excess above the background obtained by the second method is 6.9, 4.9, 3.8, and 2.9 S.D., respectively. There is also a small peak in the mass region of 2225 MeV/ c^2 (2.2 S.D.).

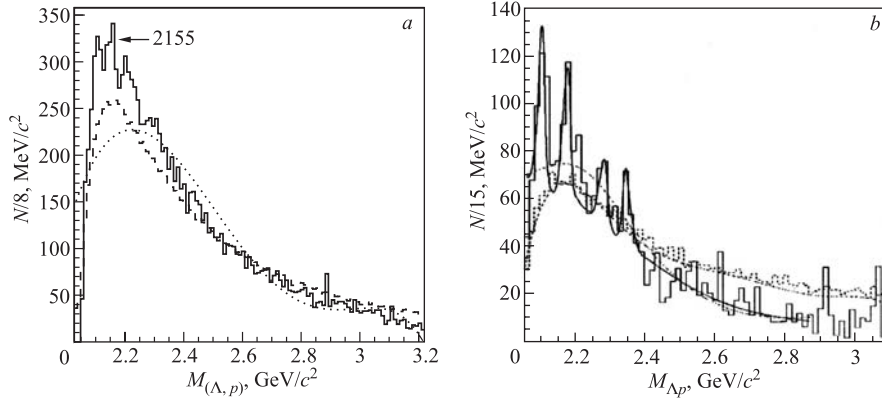


Fig. 8. *a*) The Λp spectrum for all combinations; *b*) the Λp spectrum with identified protons in the momentum range of $0.35 < P_p < 0.90$ GeV/ c . The dashed histogram is events simulated by FRITIOF model. The dashed curve is the experimental background

Figure 9, *a* shows the invariant mass of 4669(Λp) combinations with the bin size of 15 MeV/ c^2 for stopped protons in the momentum range of $0.14 < P_p < 0.30$ GeV/ c . The dashed curve is the sum of the eight-order polynomial and 4 Breit–Wigner curves with $\chi^2 = 30/25$ from fits (Table 5). The significant peak in the mass range of 2220 MeV/ c^2 (6.1 S.D.), $B_K = 120$ MeV was specially stressed by Prof. T. Yamazaki at « μ CF2007», Dubna, June 19, 2007 that is conformed by the KNC model [35] prediction by channel $K^- pp \rightarrow \Lambda p$.

The Λp effective mass distribution for 4523 combinations with relativistic protons over a momentum of $P > 1.5$ GeV/ c is shown in Fig. 9, *b*, where undivided (ΛK_s^0) are removed. The solid curve is the six-order polynomial function ($\chi^2/\text{n.d.f.} = 271/126$). The background for analysis of the experimental data is based on FRITIOF and the polynomial method. There are significant enhancements in the mass regions of 2150 (4.4 S.D.), 2210 (3.8 S.D.), 2270 (3.4 S.D.), 2670 (3.1 S.D.), and 2900 (3.1 S.D.) MeV/ c^2 . The observed peaks for the combinations with relativistic protons $P > 1.5$ GeV/ c agree with the peaks for the combination with identified protons and with stopped protons (Table 5).

Figure 10, *a, b* shows 1945 combinations for the Λp spectrum over the momentum range $0.3 < P_p < 0.95$ GeV/ c with the bin sizes of 15 and 18 MeV/ c^2 where the background from π^\pm and undivided (ΛK_s^0) combinations is removed. The upper dashed curve is the sum of the background obtained by the polynomial method and 2 BW functions (Fig. 10, *a*). The dashed curve in Fig. 10, *b* is a six-order polynomial function with $\chi^2/\text{n.d.f.} = 149/68$. There are statistical significance signals from Fig. 9, *a, b* in the mass regions of 2100 (4.0 S.D.) and 2165 (4.7 S.D.) MeV/ c^2 . The peak at 2175 MeV/ c^2 shifted to 2165 at the bin

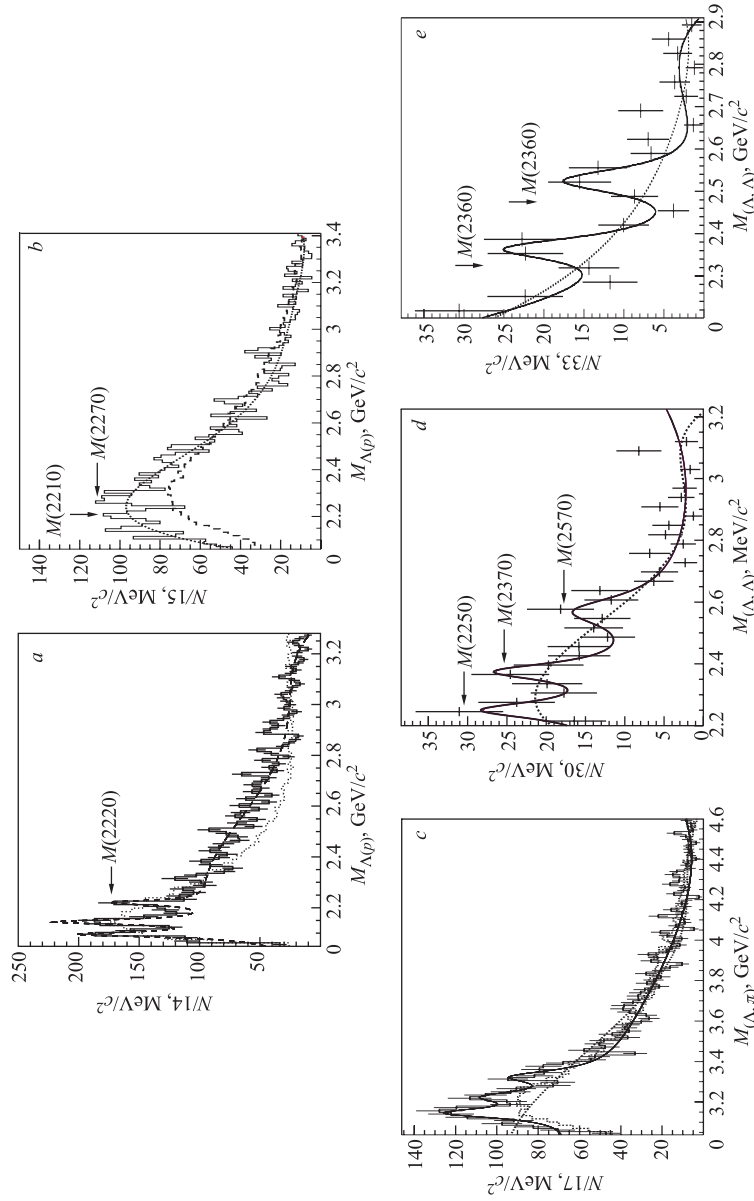


Fig. 9. a) The Λp spectrum with stopped protons in the momentum range of $0.14 < P_p < 0.30$ GeV/c; b) the Λp spectrum for relativistic positive tracks in the range of $P_p > 1.5$ GeV/c; c) the Λpp spectrum for identified protons $P_p < 0.9$ GeV/c; d) the $\Lambda\Lambda$ spectrum for 200 combinations with the bin size of 30 MeV/c²; e) the $\Lambda\Lambda$ spectrum for 137 combinations without undivided ΛK_s^0 events. The dashed histogram is events simulated by FRITIOF. The dashed curve is the experimental background

Table 5. Effective mass, width (Γ) and S.D. for exotic strange resonances observed in $p + \text{propane}$ collisions

Collisions	M (res.), MeV/c^2	Γ , MeV/c^2	S.D.
Λp	2100	24	5.7
	2150	19	5.7
	2220	23	6.1
	(2270) 2310	30	3.7
	2380	32	3.5
Λpp	3145	40	6.1
	3225	50	3.3
	3325	53	4.8
$\Lambda\Lambda$	2365	55	4.5
	2525	63	3.0
$K_s^0 p$	1540	9.2	5.5
	1613	16.1	4.8
	1821	28.0	5.0
ΛK_s^0	1750	14 ± 6	5.6
	1795	26 ± 15	3.3
$K_s^0 \pi^\pm$	885	48	6.0–8.2
	780–800	10	2.5–4.2
	720–730	≥ 30 –135	4.1–15.2
	1060	—	4.1

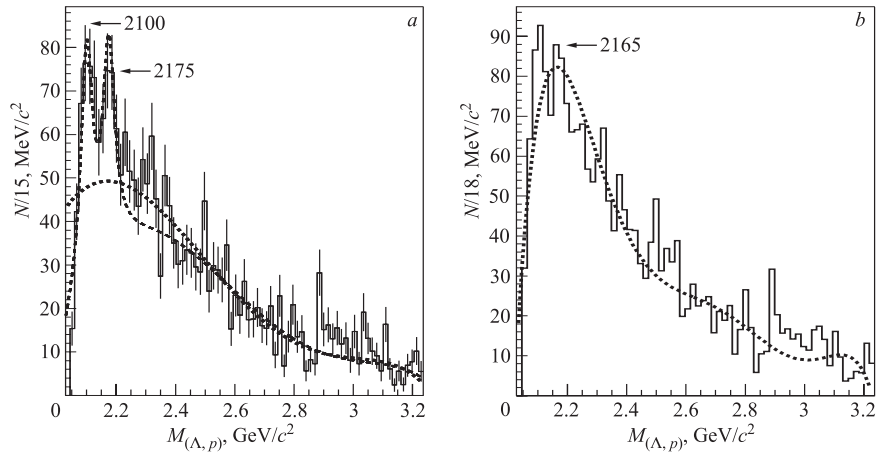


Fig. 10. *a*) Λp 1945 combinations over the momentum range of $0.3 < P_p < 0.95 \text{ GeV}/c$ with the bin sizes of 15 and 18 MeV/c^2 without π^\pm and undivided (ΛK_s^0). The dashed curve is the experimental background

size of $18 \text{ MeV}/c^2$ in Fig. 10, *b*. There are small enhancements in the mass regions of 2310 (2.7 S.D.), 2380 (2.2 S.D.), 2500 (2.3 S.D.), and 2880 (5.5 S.D.) MeV/c^2 (Fig. 10, *b*).

The Λpp effective mass distribution for 3401 combinations for identified protons with a momentum of $P_p < 0.9 \text{ GeV}/c$ is shown in Fig. 9, *e* [27–29]. The dashed curve is the six-order polynomial function ($\chi^2/\text{n.d.f.} = 245/58$, Fig. 9, *e*). In this case the analysis of the experimental data is based on the background obtained by the FRITIOF and the polynomial method. There is a significant enhancement in the mass regions of $3145 \text{ MeV}/c^2$ (6.1 S.D.) (with width $40 \text{ MeV}/c^2$). There are small enhancements in the mass regions of 3225 (3.3 S.D.), 3325 (5.1 S.D.), 3440 (3.9 S.D.), and 3652 (2.6 S.D.) MeV/c^2 (Table 5). These peaks from the Λp and Λpp spectra were partly conformed with experimental results from FOPI (GSI), FINUDA (INFN), OBELIX (CERN), and E549 (KEK).

4.1. The Simulated (Λ, p) Spectra in the $p + \text{C}$ Collision at $4.5 \text{ GeV}/c$. The inclusive cross sections are $\approx 2.2 \text{ mb}$ for Λ and $\approx 20 \mu\text{b}$ for (Λ, p) productions at $4.5 \text{ GeV}/c$ for $pC \rightarrow \Lambda X$. There are $2 \cdot 10^6$ background events of the $pC \rightarrow \Lambda pX$ reaction simulated by the FRITIOF and 150 signal events simulated by GENBODY for the resonance of $M_{\text{res}} = 2095 \text{ MeV}/c^2$. The number of Λ s is 20135 (Fig. 11, *a*). The experimental effective mass resolution is $\Delta M_{\text{res}}/M_{\text{res}} = 0.5\%$. There is not a signal for $(\Lambda, \text{pos. tracks})$ combinations. The significant signal (4.5 S.D.) is observed only for the (Λ, p) combination with the cut of momentum $0.3 < p_p < 1.0 \text{ GeV}/c$. The peak is observed in the background distribution in the mass region of $M(2140)$ which is interpreted as reflection from the well-known $\Sigma^{*+}(1385)$ resonance (Fig. 11, *b*).

4.2. The Simulated (Λ, p) Spectra for the $p + \text{D}$ Collision at $30 \text{ GeV}/c$. The inclusive cross sections are $\approx 5.4 \text{ mb}$ for Λ and $\approx 40 \mu\text{b}$ for (Λ, p) productions in the $p + \text{D}$ reaction at beam momentum $30 \text{ GeV}/c$. There are 10^6 background events of the $pC \rightarrow \Lambda X$ reaction simulated by the FRITIOF and 800 signal events simulated by GENBODY for the resonance of $M_{\text{res}} = 2095 \text{ MeV}/c^2$. The number of Λ s is 107600 (Fig. 11, *c*). The experimental invariant mass resolution is $\Delta M_{\text{res}}/M_{\text{res}} = 1\%$. Figure 11, *d* shows $(\Lambda, \text{pos. tracks})$ combinations over the mass range $4 < p < 10 \text{ GeV}/c$, where π^+ and K^+ combinations are removed. There is not a signal from the simulated resonance for $(\Lambda, \text{pos. tracks})$ in Fig. 11, *c, d*. Figure 11 *e, f* shows a signal only for (Λ, p) combinations only. There is a significant signal in the mass range of $2095 \text{ MeV}/c^2$ in Fig. 11, *e* which increases over the momentum range of $4 < p_p < 10 \text{ GeV}/c$ (Fig. 11, *f*).

4.3. (Λ, Λ) Spectra. Figure 9, *f* shows that there is a significant enhancement in the mass region of 2370 (4.5 S.D.) MeV/c^2 for the Λ, Λ spectrum (201 combinations). This peak agrees with theoretical predictions and with the earlier published result from neutron exposure by the PBC method and very poor statistics, too. There is negligible enhancement in the mass ranges of 2250, 2530,

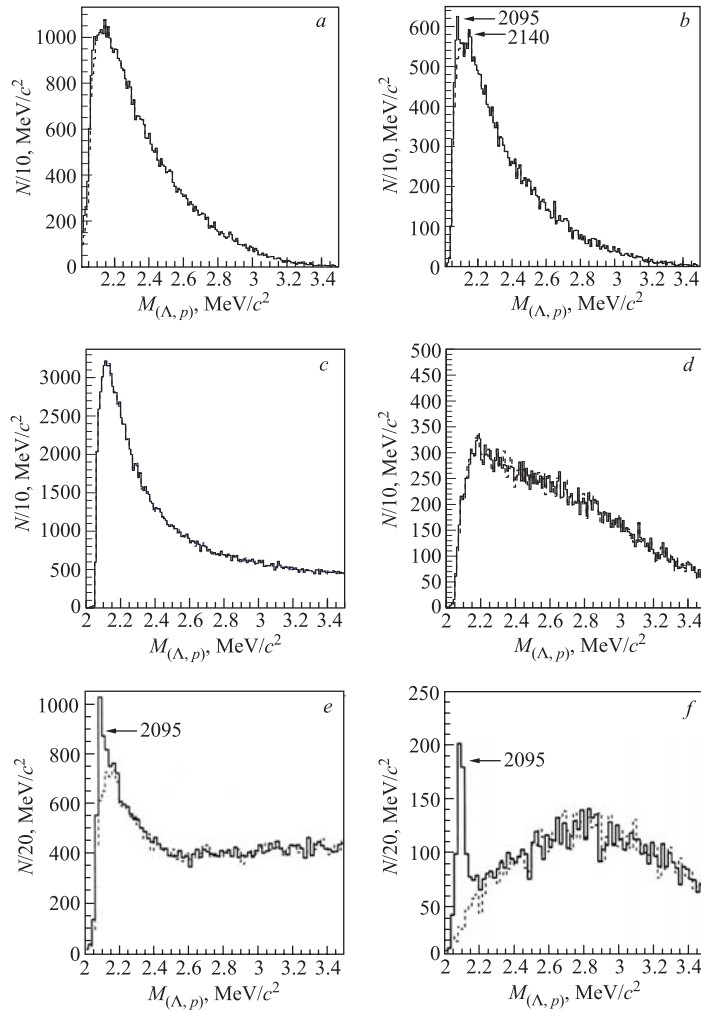


Fig. 11. *a*) The (Λ, p) invariant mass distribution for the $p + C$ reaction at 4.5 GeV/c simulated by FRITIOF model; *b*) the simulated (Λ, p) spectrum over the momentum range of $0.3 < P_p < 1.0$ GeV/c for the $p + C$ reaction at 4.5 GeV/c; *c*) the $(\Lambda, \text{pos. track})$ spectrum for $p + D$ reaction at the beam momentum of 30 GeV/c simulated by FRITIOF model; *d*) the simulated $(\Lambda, \text{pos. track})$ spectrum over the momentum range of $4 < P_p < 10$ GeV/c for the $p + D$ reaction at the beam momentum of 30 GeV/c; *e*) the simulated (Λ, p) spectrum for $p + D$ reaction at beam momentum of 30 GeV/c; *f*) the simulated (Λ, p) spectrum over the momentum range of $4 < P_p < 10$ GeV/c for the reaction $p + D$ at the beam momentum of 30 GeV/c. The solid histogram is the sum of the simulated background (dashed line) and the signal from the resonance

and $2612 \text{ MeV}/c^2$ (3.0 S.D.), too (Table 5). Figure 9, *g* shows the same distribution for 137 (Λ, Λ) combinations where undivided ΛK_s^0 events are removed. Figure 9, *g* shows that there are not signals in the mass ranges of 2250 and $2612 \text{ MeV}/c^2$.

4.4. (Λ, π^+, π^-) Spectra. The $\Lambda\pi^+\pi^-$ effective mass distribution for all 6483 combinations with the bin sizes 24 and $13 \text{ MeV}/c^2$ is shown in Fig. 12, *a, b*. The dashed curve and dashed histogram are backgrounds obtained by the polynomial function and FRITIOF methods, respectively. There are significant enhancements in the mass regions of $\Lambda^*(1750)$ (4.2 S.D., $\Gamma_e = 78, \Gamma \approx 54 \text{ MeV}/c^2, \Delta M = 24 \text{ MeV}/c^2$) and $\Lambda^*(1830)$ (5.6 S.D., $\Gamma_e = 76, \Gamma \approx 51 \text{ MeV}/c^2$). There are small enhancements in the mass regions of 1530 (2.6 S.D.), 1600 (3.1 S.D.), 1830–1860 (3.0 S.D.), (1930–1940), 2030, and $2250 \text{ MeV}/c^2$ which can be interpreted as a reflection from the resonances of $\Lambda^*(1520), \Lambda^*(1600), \Lambda^*(1750), \Lambda^*(1850)$ and $\Xi^*(1830) (\rightarrow \Lambda \bar{K}_s^0), \Sigma^*(1940)$ (and $\Xi^*(1950) \rightarrow \Lambda \bar{K}_s^0, \Sigma^*(2030)$ (and $\Xi^*(1950) \rightarrow \Lambda \bar{K}_s^0$), and $\Sigma^*(2250)$ from PDG.

Figure 12, *c, d* shows the $\Lambda\pi^+\pi^-$ effective mass distribution for 3618 combinations with bin sizes 19 and $14 \text{ MeV}/c^2$ at $P_p < 0.6 \text{ GeV}/c$. In the restricted interval $P_p < 0.6 \text{ GeV}/c$, from positive tracks combinations for the $\Lambda\pi^+\pi^-$ spectrum there remained only combinations from π^+ . The statistical significance from the signals in Fig. 12, *a, b* decreases for the same mass regions. In Fig. 12, *c* there is a significant signal in the mass range of $\Lambda^*(1600)$ (4 S.D.). Figure 12, *c* with the bin size $14 \text{ MeV}/c^2$ shows that there are not significant signals from the well-known resonances in this case.

The $\Lambda\pi^+\pi^-$ effective mass distribution for 3476 combinations with the bin size of $36 \text{ MeV}/c^2$ is shown in Fig. 12, *c* without undivided Λ, K_s^0 events. The dashed curve is the background obtained by the polynomial method. There is significant enhancement in the mass region of $\Lambda^*(1600)$ (5.5 S.D., $\Gamma_e = 80 \text{ MeV}/c^2, \Delta M = 24 \text{ MeV}/c^2$) with the width 56 (from the PDG). There are small enhancements in the mass regions of $\Lambda^*(1520)$ (3.5 S.D.), $\Lambda^*(1690)$ (3.8 S.D.), and $\Lambda^*(1800)$ (2.8 S.D.) MeV/c^2 which are interpreted as a reflection from the resonances $\Lambda^*(1520), \Lambda^*(1690),$ and $\Lambda^*(1800)$ from the PDG.

There are not observed exotic states which were earlier observed and published for $\Lambda\pi^+\pi^+$ spectrum (in the mass ranges of 1704, 2071, $2604 \text{ MeV}/c^2$) with small statistics in neutron exposure by PBC method [31, 32].

4.5. (Λ, p, π^-) Spectra. In Fig. 12, *f* the (Λ, p, π^-) effective mass distribution for 3892 combinations for identified protons in the momentum range of $P < 0.9 \text{ GeV}/c$ with the bin size $32 \text{ MeV}/c^2$ can be fitted by the six-order polynomial function which is satisfactorily described by the experimental data with $\chi^2/(\text{n.d.f.}) = 1$. The FRITIOF model background does not describe the experimental distribution. The sum of BW and FRITIOF model background with the mean mass of $2520 \text{ MeV}/c^2$, experimental width $\approx 220 \text{ MeV}/c^2$, satisfactorily describes the experimental data for the $\Lambda p\pi^-$ effective mass distribution, too.

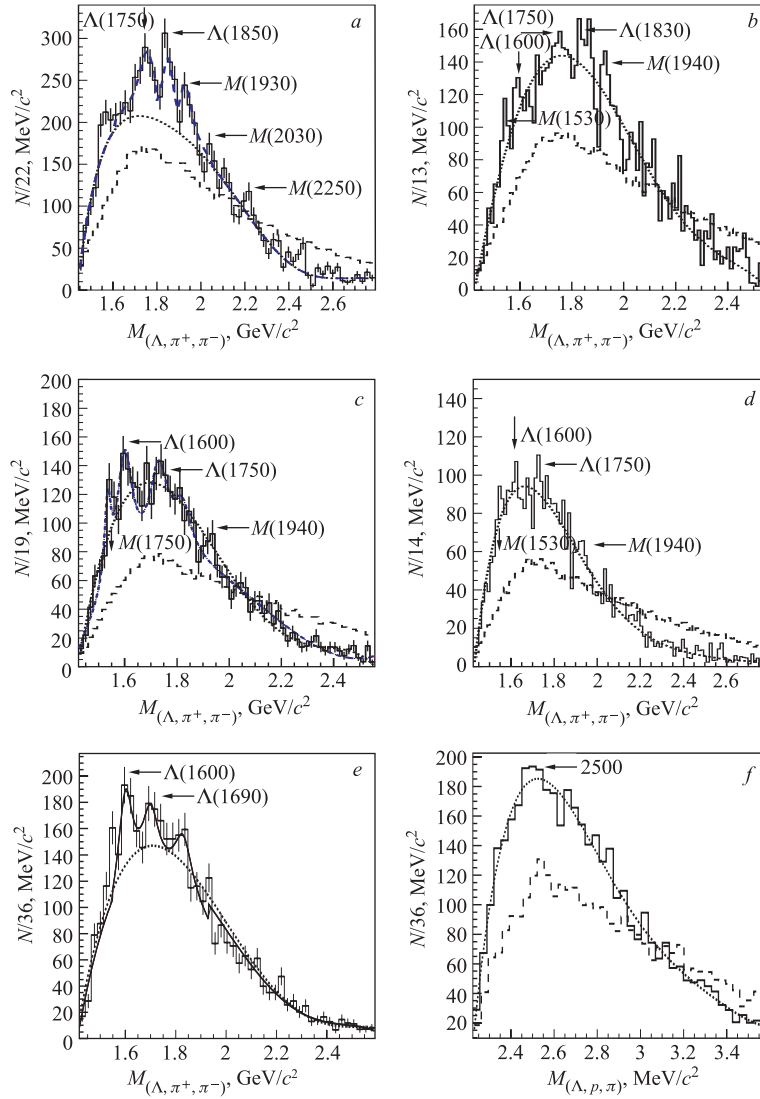


Fig. 12. *a, b*) The $\Lambda\pi^+\pi^-$ spectra over the momentum range of $P_{\pi^+} < 1 \text{ GeV}/c$ with the bin sizes of 22 and 13 MeV/c^2 , respectively; *c, d*) the $\Lambda\pi^+\pi^-$ spectra over the momentum ranges of $P_{\pi^+} < 0.6 \text{ GeV}/c$ with the bin sizes of 19 and 14 MeV/c^2 , respectively; *e*) the $\Lambda\pi^+\pi^-$ spectrum for the data [30] in the momentum range of $P_{\pi^+} < 0.9 \text{ GeV}/c$ and without undivided (Λ, K_s^0); *f*) the $\Lambda p\pi^-$ spectrum over the momentum range of $P_p < 0.9 \text{ GeV}/c$ with the bin size of 36 MeV/c^2 . The dashed histogram is the events simulated by FRITIOF. The dashed curve is the experimental background

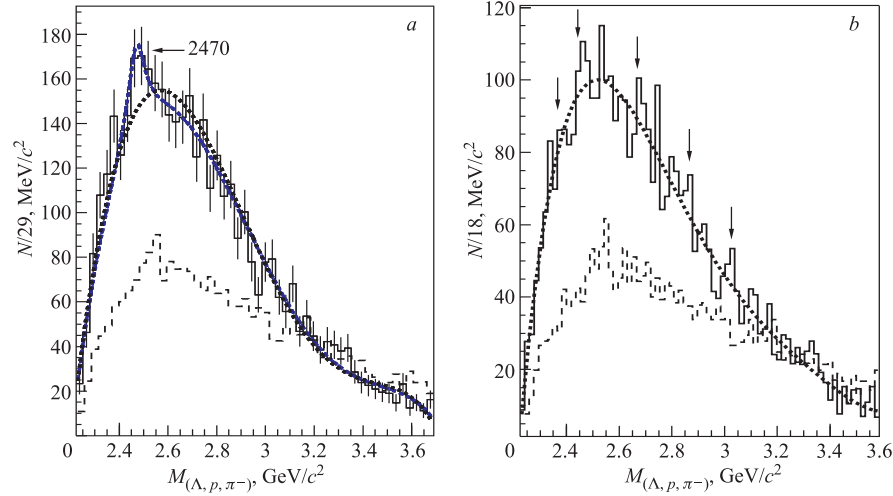


Fig. 13. *a*) The $\Lambda p\pi^-$ spectrum over the momentum range of $P_p < 0.9$ GeV/ c with the bin sizes of 29 and 18 MeV/ c^2 . The dashed curve is the experimental background

Therefore, one of probable interpretations of this peak can be a reflection from phase space distribution, too. The earlier published observation [34] of the resonance with the mass 2495 MeV/ c^2 and width 200 MeV/ c^2 for the $\Lambda p\pi^-$ spectrum by the PBC method from neutron exposure (7 GeV/ c) is not uniquely confirmed. In Fig. 12, *f* there is small enhancement in the mass range of 2670 MeV/ c^2 .

In Fig. 13, *a* there is small enhancement in the mass range of 2470 MeV/ c^2 (3.6 S.D.) with the experimental width 90 MeV/ c^2 and the bin size of 29 MeV/ c^2 . The upper dashed curve is the sum of the background obtained by the polynomial method and 1 BW function by $\chi^2/\text{n.d.f.} = 54/52$ (Fig. 13, *a*). This bin size is approximately consistent with the experimental resolution. Figure 13, *b* shows the same experimental distribution with the bin size 18 MeV/ c^2 . In this case, Fig. 13, *b* shows only negligible signals in the mass range of 2380, 2470, 2520, 2670, 2800–2860, and 3050 MeV/ c^2 . Figure 13, *b* confirms the peak in the mass range of 2670 from Fig. 12, *f*, too. Figure 13, *b* shows that the FRITIOF-simulated and experimental events have the statistical enhancement in the mass range of 2520–2540 MeV/ c^2 . Therefore, it can be interpreted as reflection from background.

4.6. The Procedure of Search for $S = -2$ H^{0+} Dihadron Events. A simple consideration of symmetry and properties of colour-magnetic interactions argues in favor of increasing binding in three-flavor matter-systems containing u , d , and s quarks. These objects are known as H particles ($uuddss$) [68–135]. Theoretical and experimental searches for H dibaryon are shown in Table 6 and in Fig. 14

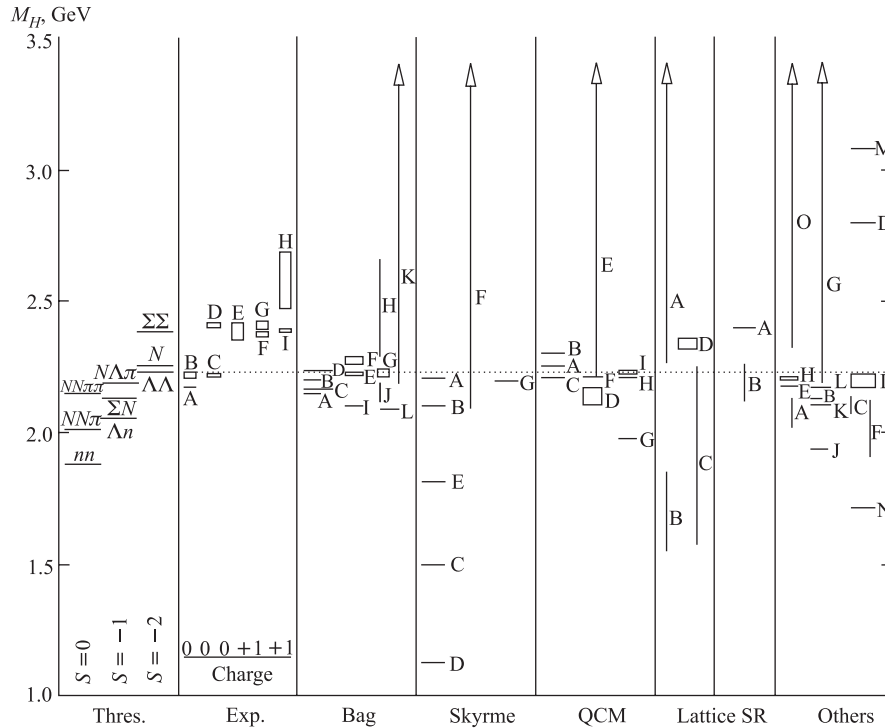


Fig. 14. The calculated masses of the H dibaryon. The dotted line indicates the $\Lambda\Lambda$ threshold. Some thresholds [134] (Thres.) and experimental masses (Exp.) of the H -dibaryon candidates reported so far are also shown. Vertical lines above the $\Lambda\Lambda$ threshold mean that the upper limits are not shown in the literature. Corresponding references are as follows. Experiment (Exp.): A — [138], B — [139, 142], C — [147], D–G — [140, 143], H, I — [144–146]. The events D–I are claimed to be excited states. Bag model (Bag): A — [68], B — [69], C — [69], D — [72], E — [73], F — [74], G — [75], H — [76], I — [77], J — [78], K — [79], L — [80]. Skyrme model (Skyrme): A — [81], B — [81], C — [82], D — [133], E — [83], F — [86], G — [87]. The value in [85] is 3.9–4.4 GeV. Non-relativistic quark cluster model (QCM): A — [88], B — [89], C — [91], D — [92], E — [93, 94], F — [95], G — [96], H — [97], I — [98]. Lattice gauge theory (Lattice) — A — [99], B — [100], C — [100], D — [101]. QCD sum rule (SR): A — [102], B — [103]. Others: A — [104], B — [105], C — [131], D — [106], E — [107], F — [108], G — [77], H — [109], I — [110], J — [111], K — [112], L — [113], M — [114], N — [116], O — [117]. Here we cite the values in the references as they are. Some of them are better to be compared with the mass of two Λ s calculated in the same framework. When the cited value is the binding energy, it is subtracted from the experimental value of the $\Lambda\Lambda$ threshold (2231 MeV). For further details see each reference

Table 6. Experimental searches for the H^0 dihyperon. For some of the experiments, we show in the third column to what range of the $H^{0,+}$ -dibaryon mass the experiment is sensitive. For KEK E224, (pp) and (p) are a proton pair and a proton in ^{12}C , respectively. $B_H = 2M_\Lambda - M_H$

Collaboration	Reaction process (production/decay)	Sensitive mass range
BNL E703 [136]	$p + p \rightarrow K^+ + K^+ + X$	$M_H = 2.0\text{--}2.5 \text{ GeV}$
BNL E810 [149, 150, 167]	$\text{Si} + \text{Pb} \rightarrow H^0 + X, H^0 \rightarrow \Sigma^- p, \Lambda \pi^- p$	
BNL E813 [151–155, 166, 167, 169]	$K^- p \rightarrow K^+ \Xi^-, (\Xi^- d)_{\text{atom}} \rightarrow H^0 + n$	$-15 < B_H < 80 \text{ MeV}$
BNL E830 [168]	$K^- + {}^3\text{He} \rightarrow K^+ + H^0 + n$	
BNL E836 [153–156, 166, 167 169]	$K^- + {}^3\text{He} \rightarrow K^+ + H^0 + n$ $K^- + {}^6\text{Li} \rightarrow K^+ + H^0 + X$	$B_H = 50\text{--}380 \text{ MeV}$
BNL E864 [167, 168]	Au + Pb collision	
BNL E885 [155, 157, 158, 167]	$K^- + (p) \rightarrow K + + \Xi^-$, $(\Xi^- A)_{\text{atom}} \rightarrow H^0 + X$	
BNL E886 [159, 167]	Au + Pt collision	
BNL E888 [160–162, 167, 165]	$p + A \rightarrow H^0 + X/H^0 \rightarrow \Sigma^- p, \Lambda n$ $H + A \rightarrow \Lambda + \Lambda + A$	$M_H < 2150 \text{ MeV}$
BNL E896 [163, 167, 168]	Au + Au collision / $H^0 \rightarrow \Sigma^- p \rightarrow \pi^- np$, $H^0 \rightarrow \Lambda \pi^- p \rightarrow \pi^- p \pi^- p$; $H^0 \rightarrow \Lambda n, H^0 \rightarrow \pi^- pn$	
BNL E910 [164]	$p + A / H^0 \rightarrow \Lambda \pi p, H^0 \rightarrow \Sigma p$	
BNL STAR [165, 188]	Au + Au collision	
KEK E176 [170–172, 178]	$K^- + (pp) \rightarrow K^+ + H$ $K^- + p \rightarrow K^+ + \Xi^-, \Xi^- + (p) \rightarrow H^0$	
KEK E224 [173–178]	$K^- + (pp) \rightarrow K^+ + H^0$ $K^- + (p) \rightarrow K^+ + \Xi^-, \Xi^- + (p) \rightarrow H^0$	
KEK E248 [179]	$p + p \rightarrow K^+ + K^+ + X$	
Fermilab E791 [182]	$H^0 \rightarrow p + \pi^- + \Lambda \Lambda \rightarrow \pi p$, $H^0 \rightarrow \Lambda + \Lambda \rightarrow p + \pi^- + p + \pi^-$	
Fermilab KTeV Collab. [183]	$p + A/H^0 \rightarrow p + \pi^- + \Lambda$	$M_H = 2194\text{--}2231 \text{ MeV}$
Shahbazian et al. [138–143]	$p + {}^{12}\text{C} \rightarrow H^0(H^+) + X$ / $H^0 \rightarrow \Sigma^- + p, \Sigma^- \rightarrow \pi^- n$	
Aslanyan et al. [144–146]	$H^+ \rightarrow p + \pi^0 + \Lambda, \Lambda \rightarrow p + \pi^-$ $H^+ \rightarrow p + \Lambda, \Lambda \rightarrow p + \pi^-$	

End of Table 6.

Collaboration	Reaction process (production/decay)	Sensitive mass range
Alekseev et al. [147]	$n + A \rightarrow H^0 + X/H^0 \rightarrow p\pi^- \Lambda, \Lambda \rightarrow \pi^- p$	$M_H < 1875.1 \text{ MeV}$
DIANA Collab. [180, 181]	$\bar{p} + \text{Xe} \rightarrow K^+ H^0 X, H^0 \rightarrow \Sigma^- + p$	
Condo et al. [137]	$\bar{p} + A \rightarrow H^0 + X/H^0 \rightarrow \Sigma^- + p$	
Ejiri et al. [148]	$d \rightarrow H + \beta + \nu, {}^{10}\text{Be} \rightarrow {}^8\text{Be} + H,$ ${}^{72}\text{Ge} \rightarrow {}^{70}\text{Ge} + H + \gamma,$ ${}^{127}\text{I} \rightarrow {}^{125}\text{I} + H + \gamma,$ ${}^{127}\text{I} \rightarrow {}^{125}\text{Te} + H + \beta^+ + \nu$	
CERN NA49 [184]	Pb + Pb collision / $H \rightarrow \Sigma^- p, \Lambda\pi p$	
CERN WA89 [185]	$\Sigma^- + A \rightarrow X + H/H \rightarrow \Lambda\Lambda, N\Xi,$ $H \rightarrow \Lambda p\pi^-, \Sigma^- p, \Sigma^0 n, \Lambda n$	
CERN WA97 [186]	Pb + Pb collision CERN	
ALICE [188]	Pb + Pb collision	
CERN OPAL [187]	Z^0 decay	

from [135]. Experimental searches for stable $S = -2$ dibaryon state are going on [15, 27, 28, 135].

There are approximately 2450 positive-prong stars from secondary positive charged particles with $\Lambda, \Lambda(K_s^0)$ selected from all the experimental events in 700 000 pictures or $3.5 \cdot 10^6$ stars. To select the events from the above samples, the following criteria were used:

- 1) approximately 380 one-positive-prong secondary events with $\Lambda, \Lambda(K_s^0)$ particles;
- 2) 115 events identified by the hypothesis as protons or relativistic particles after the track break (Fig. 8, b);
- 3) 20 events with unsuccessful fits for the background hypothesis (1–8) possibly imitating these weak decays are presented in [15];
- 4) 8 events of heavily ionizing, positively charged and more massive (than the proton) secondary particles before break;
- 5) 3 events with successful fits for the dibaryon hypothesis possibly imitating weak decays.

4.7. Identification of $\Xi^- \rightarrow \pi^- \Lambda$. The candidates for Ξ^- hyperons were observed in the sample of the so-called one-negative-prong secondary events imitating a weak decay $\Xi^- \rightarrow \Lambda + \pi^-$. In these events, Λ hyperons are directed to the vertices of one-negative-prong stars, produced by negative charged particles. Eighteen events were selected by the above samples from 29% of the experimental

Table 7. Mass and momentum of the Ξ hyperon determined by weak decay channels to $\pi^- \Lambda$

Momentum of Ξ^- , GeV/c	$M_{\pi-p}$ invariant mass of Ξ^- , GeV/c ²	Mass of Ξ^- with fits, GeV/c ²	C.L. for one vertex fit, %
0.902 ± 0.037	1.312 ± 0.009	1.313 ± 0.008	89.2 (1V-2C)
0.973 ± 0.038	1.316 ± 0.008	1.315 ± 0.007	96.0 (1V-2C)
1.320 ± 0.055	1.315 ± 0.006	1.321 ± 0.009	75.3 (1V-2C)
1.298 ± 0.038	1.313 ± 0.007	1.323 ± 0.008	29.8 (1V-2C)
2.777 ± 0.335	1.315 ± 0.006	1.398 ± 0.023	6.9 (1V-2C)

material. Five from these events were identified by using the kinematic (1V-2C) fits on the decay channel hypothesis $\Xi^- \rightarrow \Lambda + \pi^-$ (Table 7). The results of the observation of $\Xi^- \rightarrow \pi^- \Lambda$ are also presented in Table 7.

The first detected event (Fig. 7, a) is formed by the beam proton producing a twelve-prong star. The appearance of the first part of the track, 4.64 cm long, with relative ionization $I/I_0 \approx 2$, suggests that it is due to a stopped, heavily ionizing, positively charged and more massive particle than the π^- .

After break of the second part of the track it is identified as π^- 24.4 cm in length with the momentum of (217.0 ± 21.4) MeV/c.

A V^0 particle 2.15 cm long is clearly seen near the star. Note that no interactions are seen in this photograph which could serve as potential V^0 emission vertices. The proton of $P_p = (642.7 \pm 15.2)$ MeV/c and the negative pion $P_{\pi^-} = (92.2 \pm 33.0)$ MeV/c, which stop in propane, are particle decay tracks. Indeed, the invariant mass of the (p, π^-) pair is (1112.4 ± 8.5) MeV/c². Thus, the V^0 can be interpreted only as a weak decay of a Λ^0 hyperon. The hypothesis of emission of this hyperon from primary interactions fails because the fit of the hypothesis gives C.L. = 0. The hypothesis of Λ -hyperon emission from the vertex kink fits well the event with $\chi^2(1V-3C) = 1.9$, C.L. = 64%, $P_\Lambda = (734.2 \pm 33.1)$ MeV/c, $\Delta p^\perp = (20 \pm 23)$ MeV/c, $\eta = 0.054$ rad. There is coplanarity with the vector p_Ξ and the plane from the vectors p_{π^-} , p_Λ , where $\Delta p^\perp = (-6.9 \pm 12.5)$ MeV/c, $\eta = 0.010$ rad.

The hypothesis of the inclusive two-body weak decay $\Xi^- \rightarrow \pi^- + \Lambda^0$, $\Lambda \rightarrow p + \pi^-$ fits the event with $\chi^2(2V-5C) = 0.46$, C.L. = 99.8%, $M_{\Xi^-} = (1313 \pm 7.7)$ MeV/c², $p_{\Xi^-} = (903.5 \pm 36.6)$ MeV/c.

There are no successful one- or two-vertex fits for other reaction sequences given in Table 8.

4.8. The Background from Accidental Coincidence Events. We have estimated the probability of accidental coincidences by the $H^+ \rightarrow p + \Lambda^0$ samples at average loading from the beam protons in the chamber. There were $\approx 2\%$ (negligible quantity) of pictures from the chamber with overload from beam protons.

Table 8. Sequences of strong reactions and weak decays presumed to be able to imitate weak decays for the candidates $S = -2$ of the Ξ^- hyperon by channel $\Xi^- \rightarrow \pi^- + \Lambda$

Process sequences	C.L. for the one- or two-vertex fits for events
$\pi^- + n \rightarrow \pi^- + \Lambda + K^0$	No fit (1V-1C)
$\pi^- + n \rightarrow \pi^- + n, n + n \rightarrow \pi^- + p + n$	No fit (2V-6C)
$K^- + n \rightarrow \pi^- + Y^0$	No fit (1V-1C)
$K^- + n \rightarrow \pi^- + \Lambda$	No fit (1V-2C)
$K^- + 2n \rightarrow \pi^- + \Lambda + n$	No fit (1V-1C)
$\bar{p} + n \rightarrow \pi^- + \pi^0, \pi^0 + n \rightarrow \pi^- + p$	No fit (2V-6C)
$K^- \rightarrow \pi^- + \pi^0, \pi^0 + n \rightarrow \pi^- + p$	No fit (2V-6C)
$\Sigma^- \rightarrow \pi^- + n, n + n \rightarrow \pi^- + p + n$	No fit (2V-6C)
$\Sigma^- + n \rightarrow \pi^- + \Lambda + n$	No fit (1V-1C)

The probability of accidental coincidences means that neutral two-prong stars per stereo picture have the effective mass of Λ which is directed to a kink of the positively charged track, identified by the hypothesis as a relativistic particle or a proton. This probability $w = w_1 w_2 w_3 w_4 w_5 w_6 < 10^{-7}$. What kind of probability per picture is included in the expression of the value for w ? They are the following:

- w_1 are the neutral two-prong stars as V^0 ;
- w_2 are positively charged tracks before the kink identified by the hypothesis as a relativistic particle or a proton or a particle heavier than proton;
- w_3 are accidental V^0 point to some star (coplanarity);
- w_4 are the stars; w_5 is accidental V^0 with the Λ mass;
- w_6 are positively charged tracks after the kink identified by the hypothesis as a proton or a relativistic particle.

4.9. The Observed Candidates for Light H^0 and Heavy $H^{0,+}$ Dihyperons.

There are two groups of events interpreted as $S = -2$ stable dibaryons (Table 9):

- a) The first group is formed of three neutral $S = -2$ stable dibaryons, the masses of which are below the $\Lambda\Lambda$ threshold.
- b) The second group is formed of neutral and positively charged $S = -2$ heavy stable dibaryons (Figs.8 and 15). The masses of all the three dibaryons coincide within the errors and are above the $\Lambda\Lambda, \Xi N, \Lambda\Sigma$ threshold.

The last candidate for $S = -2$ $H^+ \rightarrow K^- pp$ dibaryon is shown in Fig. 16, *a* [27-29]. The appearance of its first part, 15.8 cm long, with a momentum of $p_{H^+} = (1.2 \pm 0.12)$ GeV/ c and average relative ionization more than $I/I_0 > 2$ is observed. The second part is due to two stopped protons. The momentum of negative K^- is (0.56 ± 0.03) GeV/ c ($I/I_0 \approx 1.5$). The kinematic threshold does not permit ($\sqrt{s} = 1.96$ GeV/ c) imitating the reaction with

Table 9. Mass and weak decay channels from published reports for the dihyperons observed in this experiment

Decay channel	Mass H , MeV/ c^2 (dihyperon)	C.L. of fit, %	References
$H^0 \rightarrow \Sigma^- p$	2172 ± 15	99	Z. Phys. C. 1988. V. 39. P. 151.
$H^0 \rightarrow \Sigma^- p, \Sigma^- \rightarrow n\pi^-$	2146 ± 1	30	JINR Rapid. Commun. 1995.
$H_1^0 \rightarrow H^0(2146)\gamma$	2203 ± 6	51	No. 1[69]. P. 61.
$H^0 \rightarrow \Sigma^- p, \Sigma^- \rightarrow n\pi^-$	2218 ± 12	69	Phys. Lett. B. 1990. V. 235. P. 208.
$H^0 \rightarrow \Sigma^- p, \Sigma^- \rightarrow n\pi^-$	2385 ± 31	34	Phys. Lett. B. 1993. V. 316. P. 593.
$H^+ \rightarrow p\pi^0\Lambda^0, \Lambda^0 \rightarrow p\pi^-$	2376 ± 10	87	Phys. Lett. B. 1993. V. 316. P. 593.
$H^+ \rightarrow p\pi^0\Lambda^0, \Lambda^0 \rightarrow p\pi^-$	2580 ± 108	86	Nucl. Phys. B. 1999. V. 75. P. 63.
$H^+ n \rightarrow \Sigma^+\Lambda^0 n, \Lambda^0 \rightarrow p\pi^-$	2410 ± 90	6	
$H^+ \rightarrow p\gamma\Lambda^0, \Lambda^0 \rightarrow p\pi^-$	2448 ± 47	73	JINR Commun.
$H^+ \rightarrow p\pi^0\Lambda^0, \Lambda^0 \rightarrow p\pi^-$	2488 ± 48	72	E1-2001-265. Dubna, 2002.

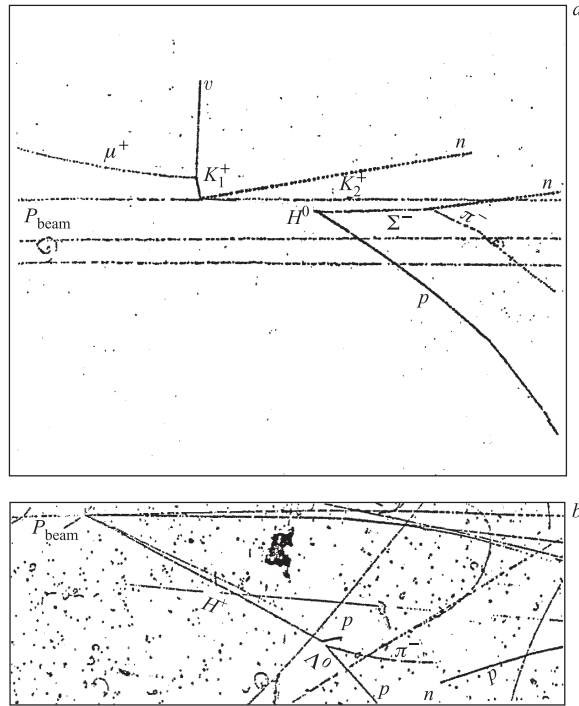


Fig. 15. a) Two-body weak decay of the heavy neutral dihyperon $H^0 \rightarrow \Sigma^0 p, \Sigma^0 \rightarrow \pi^- n$;
 b) three-body weak decay of the heavy positively charged dihyperon $H^+ \rightarrow \Lambda + p + \pi^0$,
 $\Lambda \rightarrow \pi^- p$

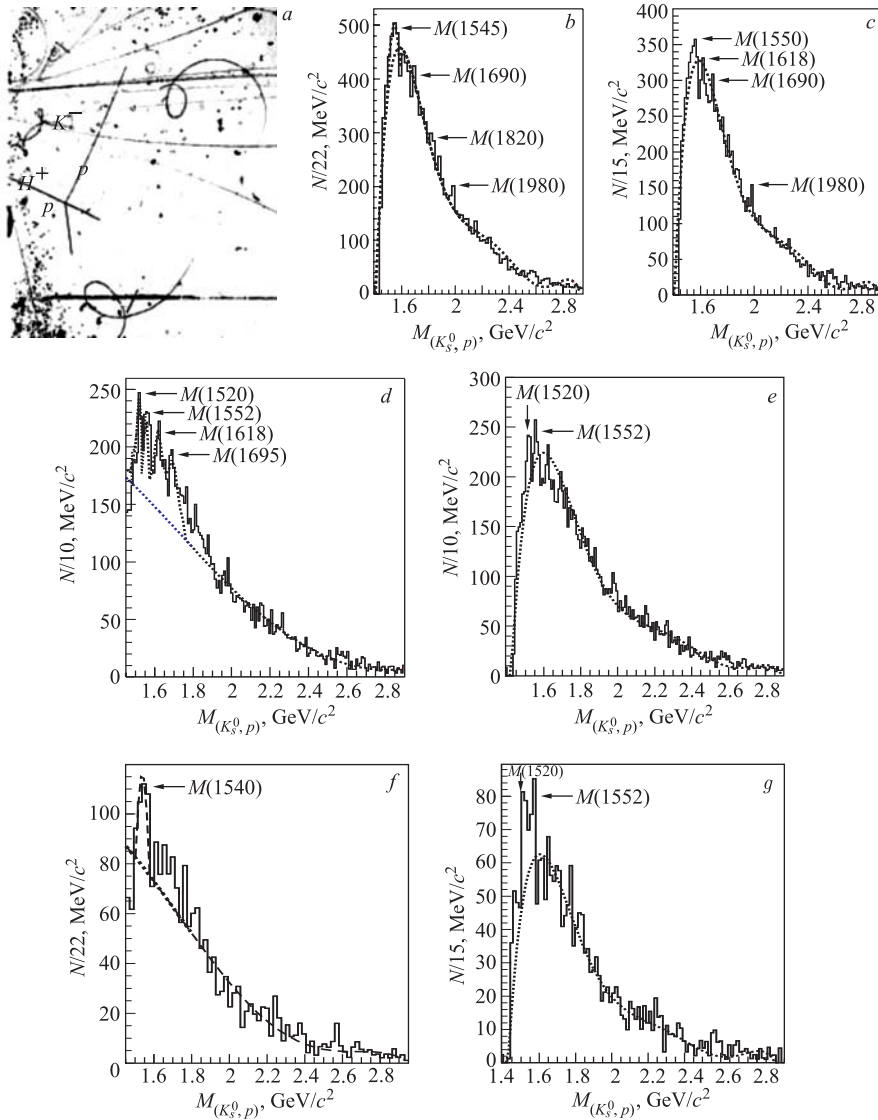


Fig. 16. *a*) The observed weak decay $H^+ \rightarrow K^- pp$. The (K_s^0, p) effective mass distribution for all 10534 combinations with the bin sizes: 22 MeV/c^2 (*b*) and 15 MeV/c^2 (*c*). The (K_s^0, p) effective mass distribution for all 10534 combinations with the bin size 10 MeV/c^2 (*d, e*). The (K_s^0, p) effective mass distribution from the reaction $p + A \rightarrow \Lambda(K_s^0 p)X$ for 1921 combinations with the bin sizes: 22 MeV/c^2 (*f*) and 15 MeV/c^2 (*g*). The dashed curves are the background obtained by the polynomial method

deuteron including Fermi motion. The $H^+ \rightarrow K^- pp$ hypothesis fits the event with $\chi^2(1V-3C) = 2.6$, C.L. = 28%, and $M_{H^+} = (2482 \pm 48) \text{ MeV}/c^2$. Also, there is fit by the hypothesis with the decay channel $H^+ \rightarrow \Sigma^+ \pi^- p$ which has much smaller probability than the above hypothesis.

5. $K_s^0 p$ SPECTRA

5.1. Preview. Several models predict the multiplet structure and characteristics of pentaquarks, for example, the chiral soliton model, the uncorrelated quark model, correlated quark models, QCD sum rules, thermal models, lattice QCD, etc. [213–226]. The recent observation of narrow, prominent exotic pentaquark baryons from antidecuplet [233] has stirred up new interest in hadron spectroscopy. The lightest member of the pentaquark antidecuplet, Θ^+ baryon predicted in [213, 215], has positive strangeness, the mass $M = 1540 \text{ MeV}/c^2$, a narrow width of $< 15 \text{ MeV}/c^2$ and spin $J^p = 1/2^+$. Jaffe and Wilczek suggested an underlying quark model structure of this state [224]. The rotational states of the $S = +1$ Θ^+ baryon are shown in [226–230]. A similar number of positive [233] and negative results have been reported in experiments on the Θ^+ .

5.2. $K_s^0 p$ Spectra for All Positive Track Combinations. Recently Θ^+ observation has been reported with the statistical significance increased for $\Theta^+ \rightarrow K_s^0 p$ to 7.3 S.D. (DIANA [235]) and 8.0 S.D. (SVD2 [236]). The results obtained from this experiment [16] are $M_{\Theta^+} = (1540 \pm 8) \text{ MeV}/c^2$, $\Gamma = (9.2 \pm 1.8) \text{ MeV}/c^2$ ($\Gamma = (9.2 \pm 0.3) \text{ MeV}/c^2$, from PDG-04). The (K_s^0 , pos. track) effective mass distribution was observed for all 10534 combinations with the bin sizes of 22 and 15 MeV/c^2 . The dashed curves (Fig. 16, *b*) are the background by the polynomial method. There is significant enhancement in the mass region 1545 (> 5 S.D., $\Gamma_e = 45 \text{ MeV}/c^2$) with the width $< 30 \text{ MeV}/c^2$. There are small enhancements in the mass regions of 1618 (3.5 S.D.), 1690 (3.8 S.D.), 1820 (4.0 S.D.), and 1980 (2.8 S.D.) MeV/c^2 , because the sum of eight-order polynomial (258/75) and 1 BW curve describes histogram by $\chi^2/\text{n.d.f.} = 229/75$ (Fig. 16, *b*). The ($K_s^0 p$) effective mass distribution (10534 comb.) with the bin size 10 MeV/c^2 is shown in Fig. 16, *d, e*. In this bin size the ($K_s^0 p$) effective mass spectrum shows significant resonant structures with $M = 1520$ (≥ 4.5 S.D., $\leq 13 \text{ MeV}/c^2$), 1552 (≥ 5.9 S.D., $\leq 15 \text{ MeV}/c^2$), 1618 (3.8 S.D., $\approx 36 \text{ MeV}/c^2$), and 1695 (3.8 S.D., $\approx 40 \text{ MeV}/c^2$). There are small enhancements in the mass ranges of 1750, 1820, and 1980 MeV/c^2 .

(K_s^0 , pos. track) spectra for 1921 combinations in reaction channel $p + A \rightarrow \Lambda(K_s^0, \text{pos. track})X$ are shown for the bin sizes 22 and 15 MeV/c^2 in Fig. 16, *f*. There is significant enhancement in the mass region 1540 (> 4.3 S.D., $\Gamma_e = 45 \text{ MeV}/c^2$) with the width $\approx 30 \text{ MeV}/c^2$. The sum of the six-order polynomial and 1 BW curve is satisfactorily described by the histogram in Fig. 16, *f*.

Figure 16, *g* with the bin size $15 \text{ MeV}/c^2$ shows that there are also small enhancements in the mass ranges of 1520 and $1552 \text{ MeV}/c^2$. The $(K_s^0, \text{pos. track})$ spectrum in the mass range of $1540 \text{ MeV}/c^2$ with the bin sizes 22 and $15 \text{ MeV}/c^2$ for all combinations restricted to the reaction channel with Λ shows the same behavior (Fig. 16).

5.3. $K_s^0 p$ Spectra with Identified Protons. The $K_s^0 p$ effective mass distribution for 2300 combinations with identified protons in the momentum range of $0.350 \leq P_p \leq 0.900 \text{ GeV}/c$ is shown in Fig. 17, *a* [16]. The solid curve is the sum of the background and 4 Breit–Wigner resonance curves. The analysis done by two methods has shown that while fitting these distributions we have the same

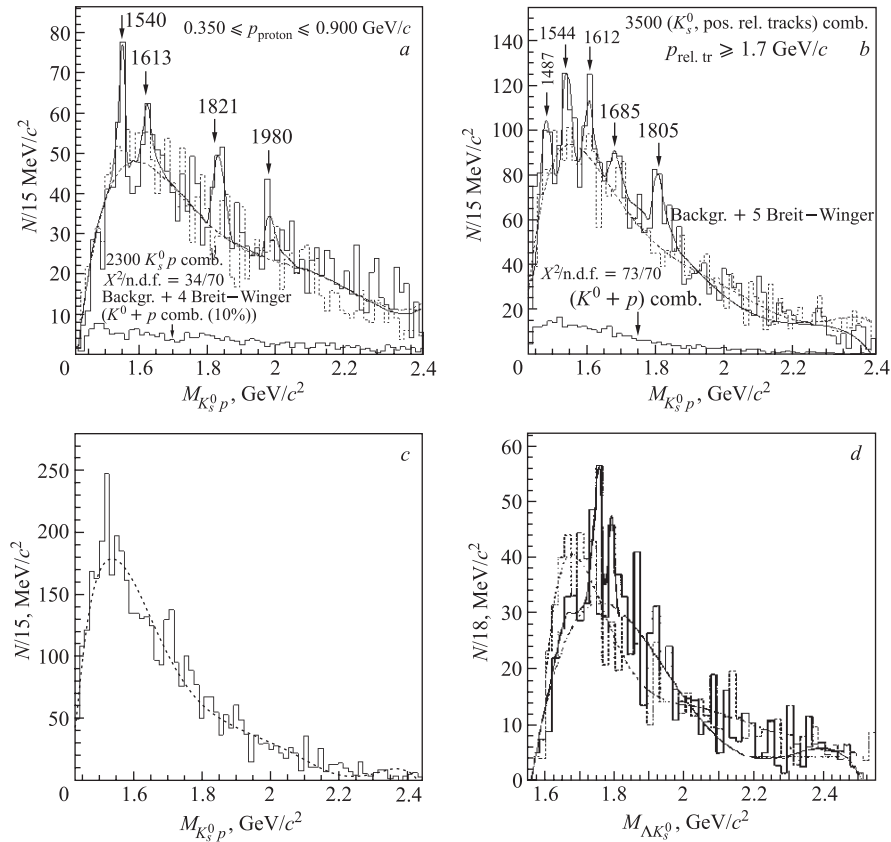


Fig. 17. *a*) The $\overline{K}_s^0 p$ spectrum for identified protons in the range of $0.35 < P_p < 0.90 \text{ GeV}/c$ ($\overline{K}^0 p$ comb. by FRITIOF — lower histogram); *b*) the $(K_s^0, \text{pos. rel. tracks})$ spectrum in the momentum range of $P_p > 1.7 \text{ GeV}/c$; *c*) the $(K_s^0, \text{pos. rel. tracks})$ spectrum in momentum range of $0.9 < P_p < 1.7 \text{ GeV}/c$; *d*) the (K_s^0, Λ) spectrum

coefficient and order of polynomial. The $K_s^0 p$ invariant mass spectrum shows resonant structures with $M_{K_s^0 p} = (1540 \pm 8), (1613 \pm 10), (1821 \pm 11) \text{ MeV}/c^2$ and $\Gamma_{K_s^0 p} = (9.2 \pm 1.8), (16.1 \pm 4.1), (28.0 \pm 9.4) \text{ MeV}/c^2$. The statistical significance of these peaks is estimated at 5.5, 4.8, and 5.0 S.D., respectively. There are also small peaks in the mass regions of 1690 (3.6 S.D.) and 1980 (3.0 S.D.) MeV/c^2 . The primary total cross section for $\Theta^+(1540)$ production in $p + \text{C}_3\text{H}_8$ interactions is estimated to be $\approx 90 \mu\text{b}$. The experimental spectrum for Θ^+ agrees with the calculated rotational spectra from the theoretical reports of D. Akers [226], V. H. Mac-Gregor, A. Nambu, P. Palazzi [228], A. A. Arkhipov [227].

The $K_s^0 p$ invariant mass distribution with the momentum $P_p > 1.7 \text{ GeV}/c$ (3500 combinations) is shown in Fig. 17, *b*. The solid curve is the sum of the background by the first method and 5 Breit–Wigner resonance curves (Fig. 17, *b*). The dashed curve is the background taken in the form of a polynomial up to the six-degree. The similarly significant enhancements for the (K_s^0 , pos. tracks) invariant mass distribution with the momentum $p_p \geq 1.7 \text{ GeV}/c$ (3500 combinations) are observed in the mass regions of 1487, 1544, 1612, and 1805 MeV/c^2 (Fig. 17, *b*) [16]. Their excess above the background is 3.0, 3.9, 3.7, and 4.0 S.D., respectively. There is a small peak in the mass region of 1685 MeV/c^2 .

5.4. (K_s^0 , pos. tracks) Spectrum at the Momentum of $0.9 \leq p_p \leq 1.7 \text{ GeV}/c$.

In Fig. 17, *c*, the (K_s^0 , pos. track) invariant mass spectrum shows resonant structures with $M = 1515$ (5.3 S.D.) and 1690 MeV/c^2 (3.8 S.D.) [16]. No obvious structure in the mass regions of 1540, 1610, and 1821 MeV/c^2 is seen in Fig. 17, *c*. The FRITIOF [12] model shows that the average multiplicity in this momentum range for all positive tracks, protons and π^+ is 1.2, 0.4, and 0.8, respectively. The background for $K_s^0 \pi^+$ and $K_s^0 K^+$ combinations is 46.6 and 4.4%, respectively. These observed peaks can be interpreted as a reflection from the resonances $\Lambda^*(1520)$ and $\Lambda^*(1700)$ in the reaction $p + \text{propane} \rightarrow K^0 \bar{K}^0 \pi^+ n p X$.

5.5. The Simulated $K_s^0 p$ Spectra at the Beam Momentum 4.5 GeV/c for Reaction pC .

The obtained by FRITIOF inclusive cross sections are $\approx 0.5 \text{ mb}$ for K_s^0 and $\approx 20 \mu\text{b}$ for $\Theta^+ \rightarrow K_s^0 p$ productions. There are $2 \cdot 10^6$ background events of the $pC \rightarrow K_s^0 X$ reaction simulated by the FRITIOF and 200 signal events simulated by GENBODY for the resonance of $M_{\text{res}} = 1540 \text{ MeV}/c^2$ (Fig. 18, *a*). The number of K_s^0 is equal to 4075. The experimental invariant mass resolution is $\Delta M_{\text{res}}/M_{\text{res}} = 1\%$. The significant signal (5.8 S.D.) was observed only by cut of positive tracks over the momentum $p_p > 0.9 \text{ GeV}/c$ in (K_s^0 , pos. tracks) combination in Fig. 18, *b*. The positive particles for simulated events over the momentum range of $P_p > 0.9 \text{ GeV}/c$ are undivided. Then the significant signal in the mass region 1530 (8.2 S.D.) MeV/c^2 was observed only for all combinations with protons in Fig. 18, *c*. The (K_s^0 , p) invariant mass distribution (dashed histogram) shows the signal in the mass region of $M(1520) \text{ MeV}/c^2$ in Fig. 18, *c, d*. This signal is interpreted as a reflection from the well-known

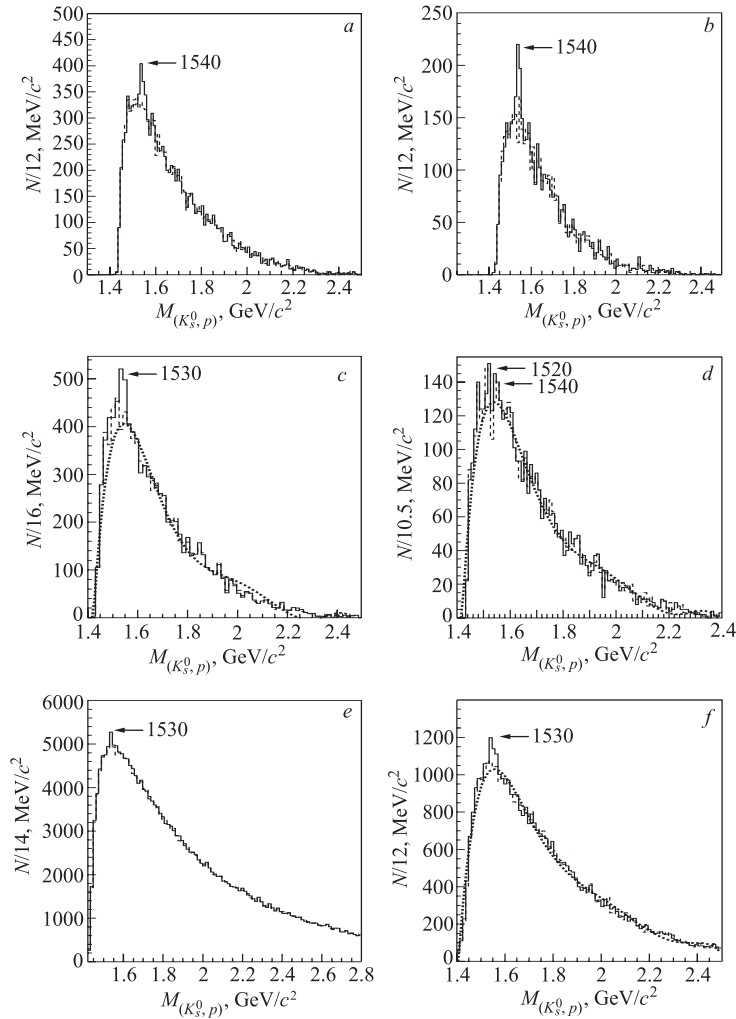


Fig. 18. *a*) The $(K_s^0, \text{pos. track})$ spectrum simulated by FRITIOF and GENBODY (signal) at the momentum 4.5 GeV/c for the reaction $p + C$; *b*) the simulated $(K_s^0, \text{pos. track})$ spectrum at the momentum 4.5 GeV/c over the momentum range of $P_p > 0.9$ GeV/c for pos. tracks; *c*) the (K_s^0, p) spectrum simulated by FRITIOF and GENBODY at the momentum 4.5 GeV/c for the reaction $p + C$; *d*) the simulated (K_s^0, proton) spectrum at the momentum 4.5 GeV/c over the momentum range of $P_p < 1$ GeV/c for protons; *e*) the $(K_s^0, \text{pos. tracks})$ spectrum simulated by FRITIOF and GENBODY at the momentum 30 GeV/c for the reaction $p + D$; *f*) the simulated $(K_s^0, \text{pos. tracks})$ spectrum at the momentum 30 GeV/c over the pos. tracks momentum range of $4 < P_p < 12$ GeV/c. The dashed curves are the polynomial function

$\Lambda^*(1520) \rightarrow \bar{K}^0 n$ resonance. There is no a signal from the simulated $\Theta(1540)$ in the (K_s^0, p) invariant mass distribution after the cut of the momentum of protons $P_p < 1$ GeV/c in Fig. 18, *d* because the main part of protons from the decay of $\Theta(1540) \rightarrow K_s^0 p$ has momentum range over $P_p > 1$ GeV/c which is larger than the average momentum of $P_{K_s^0}$. Figure 18, *d* shows reflections from Λ^* resonances, too.

5.6. $K_s^0 p$ Simulated Spectra at Beam Momentum 30 GeV/c for pD Reaction. The inclusive cross sections are ≈ 4.2 mb for K_s^0 and ≈ 40 μb for $\Theta^+ \rightarrow K_s^0 p$. There are $2 \cdot 10^6$ background events of the $pC \rightarrow K_s^0 X$ reaction simulated by the FRITIOF and 800 signal events simulated by GENBODY for the resonance of $M_{\text{res}} = 1540$ MeV/c². The number of K_s^0 is 84351 (Fig. 18, *e*). The experimental invariant mass resolution is $\Delta M_{\text{res}}/M_{\text{res}} = 1\%$. There is no signal in Fig. 18, *e* for $(K_s^0, \text{pos. tracks})$ combinations. The important part of the momentum distribution with K^+ and π^+ has a momentum smaller than 4 GeV/c. The significance signal (5.5 S.D.) with 1530 MeV/c² for the invariant mass spectrum of $(K_s^0, \text{pos. tracks})$ combination was observed only with the cut of momentum for positive tracks in $4 < P_p < 12$ GeV/c (Fig. 18, *f*). The analysis of the simulated spectrum of $(K_s^0, \text{pos. tracks})$ at the momentum 30 GeV/c revealed a shift to low masses of the $\Theta^+(1530)$ as in the report from SVD2 Collaboration because phase space has the same maximum in the mass range of 1530 MeV/c².

5.7. ΛK_s^0 Spectrum. Figure 17, *d* shows the invariant mass of 1012(ΛK_s^0) combinations with the bin size 18 MeV/c² [21]. The solid curve is the sum of the background (obtained by the first method) and 2 Breit–Wigner curves (Fig. 17, *d*). A number of peculiarities were found in the effective mass spectrum of the ΛK_s^0 system: 1650–1680, 1740–1750, 1785–1805, 1835–1860, and 1925–1950 MeV/c² in collision of a 10 GeV/c proton with the propane. The structure of the mass spectrum shows that significant enhancements were observed in two effective mass ranges 1750 and 1795 MeV/c². Their excess above the background obtained by the first method is 5.6 and 3.3 S.D., respectively. Similar results were obtained for the peak in the mass region 1740–1750 MeV/c² when the bin sizes 10, 11, 18, and 21 MeV/c² were used. The preliminary total cross section for $N^0(1750)$ production in $p + \text{propane}$ interactions is estimated to be ≈ 30 μb .

These peaks could be interpreted as possible candidates of two pentaquark states: the N^0 with the quark content $udsds$ decaying into ΛK_s^0 and the Ξ^0 quark content $udssd$ decaying into $\Lambda \bar{K}_s^0$.

6. $K_s^0 \pi^\pm$ SPECTRA

6.1. Preview. The study [242, 243] of vector mesons $K^{*\pm}(892)$ was carried out in pp interactions at 12 and 24 GeV/c by using the data (280 000 events) from exposure of CERN's 2-m hydrogen bubble chamber to p beams. Total inclusive

cross sections for $K^{*\pm} \rightarrow K_s^0 \pi^\pm X$ in pp interactions at the beam momentum $12 \text{ GeV}/c$ are $(0.25 \pm 0.03) \text{ mb}$ and $(0.02 \pm 0.02) \text{ mb}$ for inclusive production of K^{*+} and K^{*-} , respectively.

The scalar mesons have vacuum quantum numbers and are crucial for the full understanding of the symmetry breaking mechanisms in QCD, and presumably also for confinement [231]. Suggestions that the $\sigma(600)$ and $\kappa(800)$ could be glueballs have been made.

6.2. $K_s^0 \pi^+$ Spectra. Figure 19, *a, b* shows the effective mass distribution for all experimental 9539 ($K_s^0 \pi^+$) combinations with the bin sizes 16 and 13 MeV/c^2 [27, 28]. The average resolution in effective mass of $K_s^0 \pi$ system is $\approx 2\%$. Figure 19, *b* shows that ($K_s^0 \pi^+$) spectrum is approximated by the eighth-degree polynomial form with $\chi^2/\text{n.d.f.} = 150/105$. The upper dashed curve in Fig. 19, *a* is the sum of the background taken in the form of a polynomial up to the eighth degree and 1 BW function ($\chi^2/\text{n.d.f.} = 73/69$). There is significant enhancement in the mass range of $885 \text{ MeV}/c^2$, 9 S.D., $\Gamma \approx 48$. There are negligible enhancements in the mass regions of: 730, 780, 890, and $970 \text{ MeV}/c^2$. The cross section of $K^*(892)$ production (430 exp. events) is 0.5 mb at $10 \text{ GeV}/c$ for $p + C$ interaction. The peak in invariant mass spectrum at $M(885)$ is identified as the well-known $K^{*+}(892)$ resonance from PDG [10].

The effective mass of ($K_s^0 \pi^+$) distributions for 4469 combinations over the momentum range of $P_{\pi^+} < 1.0 \text{ GeV}/c$ with the bin sizes 31 and 13 MeV/c^2 are shown in Fig. 19, *c, d*. The ($K_s^0 \pi^+$) spectrum in Fig. 19, *c* is fitted by the sum of eighth-order polynomial form and 1 BW function which is satisfactorily described ($\chi^2/\text{n.d.f.} = 43/37$) without the mass range of $K^{*+}(892)$ ($0.75 < M_{K_s^0 \pi} < 0.98 \text{ GeV}/c^2$). The backgrounds obtained by FRITIOF or polynomial methods have approximately the same form when they were approximated by the 2 BW functions. Then significant enhancements are observed in the mass regions of 720 (7.3 S.D.) and 890 (5.5 S.D.) MeV/c^2 . Figure 19, *c* shows that the cut of $P_{\pi^+} < 1.0 \text{ GeV}/c$ signal in the mass range of $720 \text{ MeV}/c^2$ increased. Even the approximation of the ($K_s^0 \pi^+$) spectrum with the bin size 13 MeV/c^2 in Fig. 19, *d* by eighth-order polynomial was only done with $\chi^2/\text{n.d.f.} = 204/96$. There is a small narrow signal in the range of mass $780 \text{ MeV}/c^2$, with 3 S.D. (Fig. 19, *d*).

6.3. $K_s^0 \pi^-$ Spectra. Figure 19 shows the invariant mass distribution of 3148 ($K_s^0 \pi^-$) combinations with the bin sizes 34 and 18 MeV/c^2 [27, 28]. The upper dashed curve in Fig. 19, *e* is the sum of 1 BW and the background (below dashed curve) taken in the form of a polynomial up to the eighth degree ($\chi^2 = 42/36$ without the mass ranges of $K^{*-}(892)$). The backgrounds obtained by the FRITIOF or polynomial methods have approximately the same form when they were approximated with adding 2 BW functions. There are similar significant enhancements in the mass regions of 720 and $890 \text{ MeV}/c^2$ (3.1 S.D., ≈ 45 events) (Fig. 19, *e*). The signal in the mass range of $890 \text{ MeV}/c^2$ is identified as the well-known resonance $K^{*-}(892)$ from PDG. Therefore, the cross section of $K^{*-}(892)$

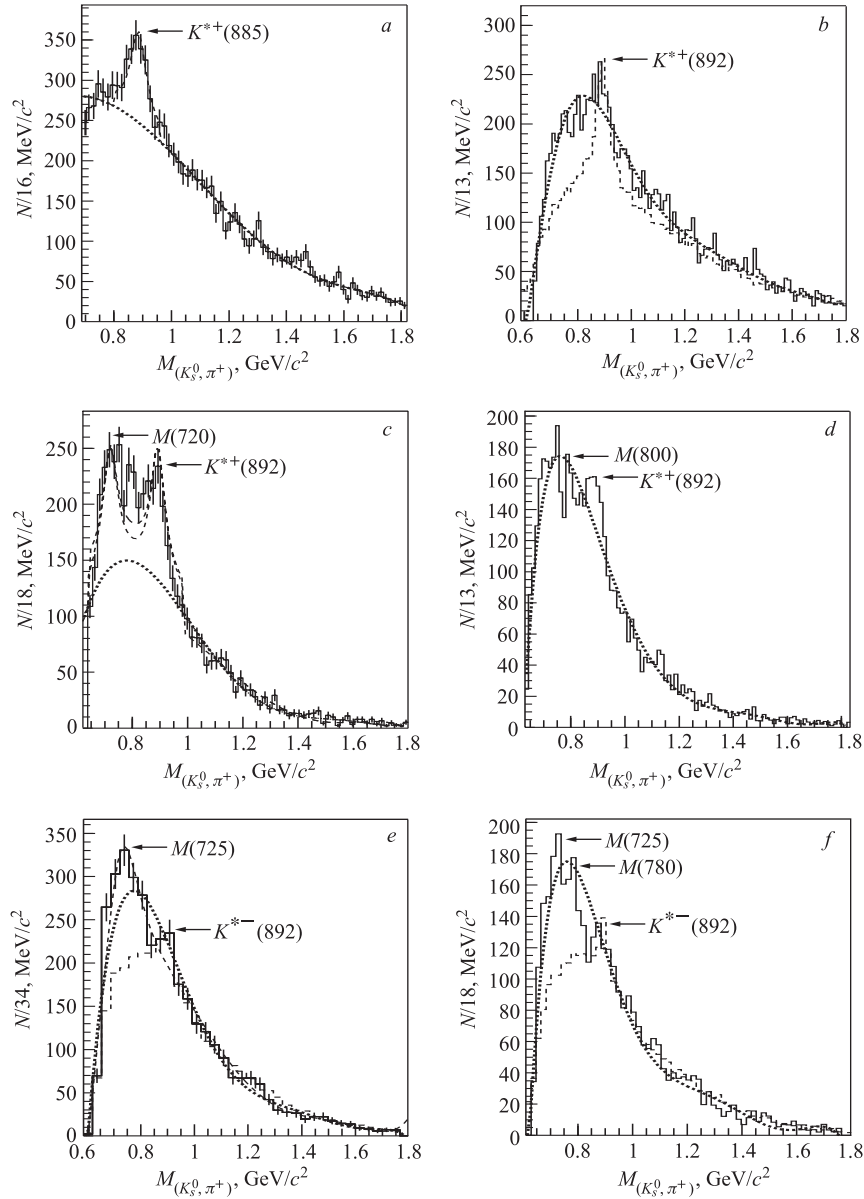


Fig. 19. The $K_s^0\pi^+$ spectrum with the bin sizes: 16 (a) and 13 MeV/c^2 (b); the $K_s^0\pi^+$ spectrum over the momentum range of $P_\pi < 1 \text{ GeV}/c$ with the bin sizes: 31 (c) and 13 MeV/c^2 (d); the $K_s^0\pi^-$ spectrum with the bin sizes: 34 (e) and 18 MeV/c^2 (f). The dashed histogram is the events simulated by FRITIOF

is approximately 10 times smaller than for $K^{*+}(892)$ in this experiment, too. Figure 19, *f* shows that the $(K_s^0\pi^-)$ spectrum is approximated by eight-order polynomial function with $\chi^2/\text{n.d.f.} = 114/65$. There are small enhancements in the mass range of 780, 980, and 1070 MeV/c^2 (Fig. 19, *f*). The preliminary total cross section for $M(720)$ in $p + \text{propane}$ interactions is larger than 30 μb .

CONCLUSION

- The experimental Λ/π^+ ratio in the $p\text{C}$ reaction is approximately two times larger than this ratio from pp reactions or from $p\text{C}$ reactions simulated by the FRITIOF model at the momentum 10 GeV/c .
- The invariant mass of the $\Lambda\pi^+$ and $K_s^0\pi^+$ spectra shows the well-known resonances from PDG as $\Sigma^{*+}(1385)$ and $K^{*\pm}(892)$ which are a good test for this method.
- The mass of excited $\Sigma^{*-}(1385)$ is shifted to $M(1370)$ in medium of carbon and its width is two times larger than the width in PDG, respectively. Particularly, such behavior can be explained as a sum of contributions from phase space in the mass range of $M(1360)$ and enhanced productions of stopped Ξ^- , $\Sigma^{*-}(1385)$ which is the medium effect in the carbon nucleus.
- The $\Sigma^{*-}(1480)$ resonance is observed, which agrees with the reports from SVD2 and COSY Collaborations.
- There are enhancement signals from all observed hyperons. The $\Lambda\pi^+\pi^-$ invariant mass spectrum shows enhancement signals from the well-known resonances from PDG.
- A number of important peculiarities were observed in the effective mass spectrum for exotic states with the decay modes (Table 5) [21–29] (Λ, π), (Λ, π^+, π^-), (Λ, p), (Λ, p, p), (Λ, Λ), (Λ, p, π^-), (Λ, K_s^0), and ($K_s^0\pi^\pm$).
- The statistical significance signals are observed in the spectrum of (Λ, p) in the momentum range of $0.15 < P_p < 0.30 \text{ GeV}/c$ for protons (Table 5).
- Particular peaks for (Λ, p) and (Λ, p, p) spectra agree with the experimental data from the reports of FOPI, E471 (KEK), OBELIX, FINUDA Collaborations (Table 4), but there is some disagreement in peak positions or widths.
- The spectrum of (K_s^0p) combinations shows peaks for Θ^+ which agree with the rotational states predicted by P. Palazzi [228], M. H. Mac Gregor [230] and Y. Nambu [229].
- In the primary $(K_s^0, \text{pos. tracks})$ spectrum the peak in the mass range of 1540 with width $\approx 30 \text{ MeV}/c^2$ can be interpreted as a sum of two peaks in the mass ranges of 1520 and 1552 MeV/c^2 with widths smaller than 15 MeV/c^2 at the bin size 10 MeV/c^2 .
- In the $(K_s^0, \text{pos. tracks})$ spectrum over the momentum range of $0.9 < P_p < 1.7 \text{ GeV}/c$ there are peaks in the mass ranges of 1520 and 1695 MeV/c^2 which can be reflections from $\Lambda^*(1520)$ and $\Lambda^*(1690)$ resonances.

- In the (Λ, K_s^0) spectrum the peaks at (1750 ± 18) and (1795 ± 20) MeV/c^2 are possible candidates for two pentaquark states: N^0 with the quark content $udsds$ decaying into ΛK^0 and the Ξ^{*0} with the quark content $udssd$ decaying into $\Lambda \bar{K}_s^0$.

- A few events were registered by the hypothesis of light H^0 and heavy $H^{0,+}$ dihyperons by weak decay channels to (Σ^-, p) and (Λ, p, π) . Recently, the dihyperon was observed by channel $H^+(2480) \rightarrow K^- pp$ (or $\rightarrow \Sigma^+ p \pi^-$).

- The analysis shows that the simulated spectra of (K_s^0, p) for the resonance $\Theta^+(1540)$ at the momenta $4.5(p + C)$ and $30(p + D)$ GeV/c shifted to $M = 1530 \text{ MeV}/c^2$, when the maximum of phase space for $K_s^0 p$ spectrum was observed in the same mass range, too.

- The analysis of the experimental and simulated data for the effect/background ratios at the momenta of 4.5, 10, and 30 GeV/c shows that at initial stage of the identification of the exotic narrow resonances it is necessary to use some kinematical restrictions for efficient separation of the necessary channels. Reactions with light nuclei (N, D, He, C) should be chosen specially for reduction of multiplicity from π^\pm and K^\pm particles.

- The $K_s^0 \pi^\pm$ invariant mass spectra show enhancement signals in the mass range of 720, 885, 980, and 1070 MeV/c^2 (Table 5). The peak in the mass range of 720 MeV/c^2 can be interpreted as a κ -scalar meson with the width $\geq (30-130) \text{ MeV}/c^2$.

- The search for and study of exotic strange multibaryon states with Λ and K_s^0 subsystems at MPD (NICA, JINR), CBM (FAIR, GSI), p07 (JPARC, KEK), OBELIX (CERN), and AMADEUS (DAFNE, INFN) can provide information about their nature, properties and will be a test for the observed PBC data. Higher-statistics experiments with the mass resolution $\approx 1\%$ are needed.

REFERENCES

1. Balandin M. et al. // Nucl. Instr. Meth. 1963. V. 20. P. 110.
2. Ti Nguen-Din et al. JINR Commun. 13-5942. Dubna, 1971.
3. Vishnevskaya K. P. et al. JINR Commun. 1-5978. Dubna, 1971.
4. Armutlijski D. A. et al. // Yad. Fiz. 1986. No. 43(2). P. 366.
5. Kladnitskaya E. N., Jovchev K. J. JINR Commun. P1-86-166. Dubna, 1986;
Arakelian S. G. et al. JINR Commun. 1-82-683. Dubna, 1982.
6. Akhababian N. O. et al. JINR Commun. D1-82-445. Dubna, 1982; Yad. Fiz. 1983. V. 37. P. 124.
7. Agakshiev G. N. et al. JINR Commun. 1-83-662. Dubna, 1983.
8. Armutlijski D. A. et al. JINR Commun. P1-86-459. Dubna, 1986; JINR Commun. P1-87-423. Dubna, 1987.

9. *Deutshman M. et al.* // Nucl. Phys. B. 1970. V. 103. P. 426.
10. *Hagiwara K. et al.* Particle Data Group // Phys. Rev. D. 2002. V. 66. P. 010001.
11. *Lyuboshits V. L. et al.* // JINR Rapid Commun. 1995. No. [74]. P. 209.
12. *Pi H. (FRITIOF)* // Comp. Phys. Commun. 1992. V. 71. P. 173;
Galoian A. S. et al. JINR Commun. P1-2002-54. Dubna, 2002; J. Nucl. Phys. 2003. V. 66, No. 5. P. 868.
13. *Barashenkov B. S., Toneev V. D.* Interactions of Particles and Nucleus with Nucleus. Atomizdat, 1972.
14. *Aslanyan P. Zh.* // Part. Nucl., Lett. 2007. V. 4, No.1(137). P. 99–108; JINR Commun. E1-2005-150. Dubna, 2005.
15. *Aslanyan P. Zh.* JINR Commun. E-2001-265. Dubna, 2001.
16. *Aslanyan P. Zh. et al.* JINR E1-2004-137. Dubna, 2004; Nucl. Phys. A. 2005. V. 755. P. 375.
17. *Aslanyan P. Z. et al.* // Proc. of the 16th Intern. Spin Physics Symp., Trieste, Italy, Oct. 10–16, 2004.
18. *Aslanyan P. Z.* // Proc. of Annual Winter School of St. Petersburg Nucl. Phys. Institute, St. Petersburg, Feb. 18–23, 2008.
19. *Aslanyan P. Z.* // Proc. of Conf. LEAP/EXA-08, Wien, Sept. 14–19, 2008.
20. *Aslanyan P. Z. et al.* // Proc. of XVII ISHEPP, Dubna, Sept. 25–30, 2004.
21. *Aslanyan P. Zh. et al.* // Part. Nucl., Lett. 2006. V. 3, No. 5(134). P. 331–334; JINR Commun. E1-2005-149. Dubna, 2005.
22. *Aslanyan P. Z.* hep-ex/0605002. 2006.
23. *Aslanyan P. Zh.* // Proc. of Conf. «I. Ya. Pomeranchuk and Physics at the Turn of Centuries», Moscow, Jan. 24–28, 2003 / Ed. by Berkov A. V., Narozhny N. B., Okun L. B. World Sci., 2003. P. 247–251; hep-ex/0406034. 2004.
24. *Aslanyan P. Z. et al.* // Proc. of Conf. LEAP05, Bonn, May 16–22, 2005; AIP. V. 796. P. 195.
25. *Aslanyan P.* // Miniproc. of the Intern. Workshop on Exotic Hadronic Atoms, Trento. 2006; hep-ph/0610201. 2006.
26. *Aslanyan P. Zh.* // Proc. Helmholtz Intern. Summer School on Dense Matter in Heavy Ion Collisions and Astrophysics, Dubna, Aug. 21 – Sept. 1, 2006; Part. Nucl. 2008. V. 39, Issue 4; hep-ex/0610086.
27. *Aslanyan P. et al.* // Proc. of XVIII ISHEPP, Dubna, Sept. 25–30, 2006; Proc. of Spin'06, Kyoto, Japan, Oct. 2–7, 2006. AIP. V. 915; hep-ex/0610086v1.
28. *Aslanyan P. Zh.* // Proc. of IUTP'07, Schladming, Austria, March 25 – April 3, 2007; Eur. Phys. J. Special Topics. 2007. V. 152.
29. *Aslanyan P. Zh.* // Proc. of Intern. Conf. on Hadron Structure, Bratislava, Sept. 2–8, 2007; Fizika B (Zagreb). 2008. V. 17. P. 1; hep-ex-0710.4322v2.

30. *Aslanyan P. Zh.* // Proc. of XII Intern. Conf. on Hadron Spectroscopy, Frascati, Oct. 8–12, 2007; 2008. V. XLVI. P. 1283; hep/ex-0710.4322v2.
31. *Shakhbazian B. A. et al.* // Nucl. Phys. A. 1982. V. 374. P. 73c–93c.
32. *Shakhbazian B. A.* JINR Commun. E1-82-446. Dubna, 1982; Intern. Conf. on Hypernuclear and Kaon Physics. Heidelberg, 1982.
33. *Shakhbazian B. A. et al.* JINR, D1-81-107. Dubna, 1981.
34. *Shakhbazian B. A. et al.* // JINR Rapid Commun. 1991. No. 2[48].
35. *Yamazaki T., Akaishi Y.* // Phys. Lett. B. 2002. V. 535. P. 70.
36. *Yamazaki T., Akaishi Y.* // Phys. Rev. C. 2007. V. 76. P. 045201.
37. *Kienle P., Yamazaki T., Akaishi Y.* // Phys. Lett. B. 2006. V. 632. P. 187.
38. *Shevchenko N. V., Gal A., Mares J.* // Phys. Rev. Lett. 2007. V. 98. P. 082301;
Shevchenko N. V. et al. // Phys. Rev. C. 2007. V. 76. P. 044004.
39. *Dote B. A. et al.* // Phys. Rev. C. 2004. V. 70. P. 044313.
40. *Akaishi Y., Dote A., Yamazaki T.* // Phys. Lett. B. 2005. V. 613. P. 140.
41. *Jido D. et al.* // Nucl. Phys. A. 2003. V. 725. P. 181;
Magas V. K., Oset E., Ramos A. // Phys. Rev. Lett. 2005. V. 95. P. 052301.
42. *Yamazaki T., Akaishi Y.* // Phys. Lett. B. 1999. V. 453. P. 1–6.
43. *Suzuki T. et al.* // Phys. Lett. B. 2004. V. 597. P. 263.
44. *Suzuki T. et al.* nucl-ex/0709.0996v2. 2007.
45. *Sato M. et al.* // Phys. Lett. B. 2007 (in press); nucl-ex/0708.2968.
46. *Garcilazo H., Fernandez-Carames T., Valcarce A.* // Phys. Rev. C. 2007. V. 75. P. 034002; V. 76. P. 034001.
47. *Samanta C., Chowdhury P. R., Basu D. N.* // J. Phys. G: Nucl. Part. Phys. 2006. V. 32. P. 363373.
48. *The AMADEUS Collab.* INFN, Frascati, LNF07/24(IR). 2007.
49. *Agnello M. et al.* // Phys. Rev. Lett. 2005. V. 94. P. 212303;
Agnello M. et al. 0708.3614v1. 2007.
50. *Iwasaki M. et al.* nucl-ex/0310018v2.
51. *Herrmann N.* // Proc. EXA05, 2006.
52. *Bendiscioli G. et al.* // Nucl. Phys. A. 2007. V. 789. P. 222.
53. *Miyano K. et al.* // Phys. Rev. C. 1988. V. 38.
54. *Anikina M. et al.* // Phys. Rev. Lett. 1971. V. 50.
55. *Albergo S. et al.* // Phys. Rev. Lett. 2002. V. 88. P. 6.
56. *Back B. et al. (E866, E917 Collab.).* nucl-ex/9910008.
57. *Ahle L. et al.* // Phys. Rev. C. 1999. V. 60; Phys. Lett. B. 2000. V. 476. P. 1.

58. *Abbott T. et al.* // Phys. Lett. B. 1991. V. 291. P. 341;
Abbott T. et al. // Phys. Rev. C. 1994. V. 50. P. 1024.
59. *Rafaelski J. et al.* // Phys. Lett. B. 1980. V. 91. P. 281; Phys. Rev. Lett. 1982. V. 48. P. 1066.
60. *Koch P., Rafaelski J., Greiner W.* // Phys. Lett. B. 1983. V. 123. C. 151.
61. *Rundrup J., Ko C. M.* // Nucl. Phys. A. 1980. V. 343. P. 519.
62. *Asai F., Sato H., Sano M.* // Phys. Lett. B. 1981. V. 98. P. 19.
63. *Cleymans J., Redlich K.* // Phys. Rev. C. 1999. V. 60.
64. *Braun-Munzinger P. et al.* // Nucl. Phys. A. 2002. V. 697. P. 902–912; Phys. Lett. B. 1995. V. 344. P. 43.
65. *Dunlop J. C., Ogilvie C. A.* // Phys. Rev. C. 2000. V. 61. P. 031901(R);
Gazdzicki M. hep-ph/0305176v2. 2003.
66. *Becattini F. et al.* // Phys. Rev. C. 2001. V. 24. P. 024901; hep-ph/0002267.
67. *Roos M. et al.* Review of Particle Properties. Particle Data Group // Phys. Lett. B. 1982. V. 111. P. 1.
68. *Jaffe R. L.* // Phys. Rev. Lett. 1977. V. 38. P. 195; 617(E);
Jaffe R. L. // Phys. Rev. D. 1977. V. 15. 267; 281.
69. *Aerts A. Th. M., Mulders P. J. G., de Swart J. J.* // Phys. Rev. D. 1978. V. 17. P. 260;
Mulders P. J., Aerts A. T., de Swart J. J. // Phys. Rev. D. 1980. V. 21. P. 2653.
70. *Kopeliovich V. B., Schwesinger B., Stern B. E.* // Nucl. Phys. A. 1992. V. 549. P. 485.
71. *Faessler A. et al.* // J. Phys. G. 2001. V. 27. P. 1851–1868; nucl-th/9912074.
72. *Liu K. F., Wong C. W.* // Phys. Lett. B. 1982. V. 113. P. 1.
73. *Mulders P. J., Thomas A. W.* // J. Phys. G: Nucl. Phys. 1983. V. 9. P. 1159.
74. *Aerts A. T. M., Rafelski J.* // Phys. Lett. B. 1984. V. 148. P. 337.
75. *Saito K.* // Prog. Theor. Phys. 1984. V. 72. P. 674.
76. *Kondratyuk L. A., Krivoruchenko M. I., Shchepkin M. G.* // Yad. Fiz. 1987. V. 45. P. 514; Sov. J. Nucl. Phys. 1987. V. 45. P. 323.
77. *Fleck S. et al.* // Phys. Lett. B. 1989. V. 220. P. 616.
78. *Golowich E., Sotirelis T.* // Phys. Rev. D. 1992. V. 46. P. 354.
79. *Maltman K.* // Phys. Lett. B. 1992. V. 291. P. 371.
80. *Dorokhov A. E., Kochelev N. I.* JINR Preprint E2-86-847. Dubna, 1986;
Dorokhov A. E., Zubov Yu. A., Kochelev N. I. // Fiz. Elem. Chast. At. Yadra. 1992. V. 23. P. 1192; Sov. J. Part. Nucl. 1993. V. 23. P. 522.
81. *Balachandran A. P. et al.* // Phys. Rev. Lett. 1984. V. 52. P. 887;
Balachandran A. P. et al. // Nucl. Phys. B. 1985. V. 256. P. 525.
82. *Jaffe R. L., Korpa C. L.* // Nucl. Phys. B. 1985. V. 258. P. 468.

83. *Kunz J., Masak D.* // Phys. Lett. B. 1987. V. 191. P. 174;
Kunz J., Mulders P. J. G. // Phys. Lett. B. 1988. V. 215. P. 449;
Mulders P. J., Kunz J. // Nucl. Phys. A. 1989. V. 497. P. 339c.
84. *Lee H. K., Kim J. H.* // Mod. Phys. Lett. A. 1990. V. 5. P. 887.
85. *Kopeliovich V. B., Schwesinger B., Stern B. E.* // Nucl. Phys. A. 1992. V. 549. P. 485.
86. *Scholtz F. G., Schwesinger B., Geyer H. B.* // Nucl. Phys. A. 1993. V. 561. P. 542.
87. *Thomas G. L., Scoccola N. N., Wirzba A.* // Nucl. Phys. A. 1994. V. 575. P. 623.
88. *Oka M., Shimizu K., Yazaki K.* // Phys. Lett. B. 1983. V. 130. P. 365; Nucl. Phys. A. 1987. V. 464. P. 700.
89. *Silvestre-Brac B., Carbonell J., Gignoux C.* // Phys. Rev. D. 1987. V. 36. P. 2083.
90. *Baldin A. M.* // Proc. of Intern. School on Nuclear Physics, Erice, March–April 1979.
91. *Straub U. et al.* // Phys. Lett. B. 1988. V. 200. P. 241;
Straub U. et al. // Nucl. Phys. A. 1990. V. 508. P. 385c;
Faessler A., Straub U. // Prog. Part. Nucl. Phys. 1990. V. 24. P. 323.
92. *Koike Y., Shimizu K., Yazaki K.* // Nucl. Phys. A. 1990. V. 513. P. 653.
93. *Takeuchi S., Oka M.* // Phys. Rev. Lett. 1991. V. 66. P. 1271.
94. *Oka M., Takeuchi S.* // Nucl. Phys. A. 1991. V. 524. P. 649.
95. *Nakamoto C., Suzukiand Y., Fujiwara Y.* // Prog. Theor. Phys. 1997. V. 97. P. 761;
Nakamoto C., Fujiwara Y., Suzuki Y. // Nucl. Phys. A. 1998. V. 639. P. 51c.
96. *Wolfe C. E., Maltman K.* // Phys. Lett. B. 1997. V. 393. P. 274.
97. *Shimizu K., Koyama M.* // Nucl. Phys. A. 1999. V. 646. P. 211.
98. *Shen P. N. et al.* // J. Phys. G. 1999. V. 25. P. 1807.
99. *Mackenzie P. B., Thacker H. B.* // Phys. Rev. Lett. 1985. V. 55. P. 2539.
100. *Iwasaki Y., Yoshie T., Tsuboi Y.* // Phys. Rev. Lett. 1988. V. 60. P. 1371;
Yoshie T., Iwasaki Y., Sakai S. // Nucl. Phys. B (Proc. Suppl.). 1990. V. 17. P. 413.
101. *Negele J. W., Pochinsky A., Scarlet B.* // Nucl. Phys. B. 1999. V. 73. P. 255.
102. *Larin S. A. et al.* // Yad. Fiz. 1986. V. 44. P. 1066; Sov. J. Nucl. Phys. 1986. V. 44. P. 690.
103. *Kodama N., Oka M., Hatsuda T.* // Nucl. Phys. A. 1994. V. 580. P. 445.
104. *Nishikawa K., Aoki N., Hyuga H.* // Nucl. Phys. A. 1991. V. 534. P. 573.
105. *Pal D., McGovern J. A.* // J. Phys. G. 1992. V. 18. P. 593.
106. *Carlson J., Pandharipande V. R.* // Phys. Rev. D. 1991. V. 43. P. 1652.
107. *Rosner J. L.* // Phys. Rev. D. 1986. V. 33. P. 2043.
108. *Goldman T.* // Phys. Rev. Lett. 1987. V. 59. P. 627.
109. *Aizawa N., Hirata M.* // Prog. Theor. Phys. 1991. V. 86. P. 429.

110. Wang F. *et al.* // Phys. Rev. C. 1995. V. 51. P. 3411.
111. Kondratyuk L. A., Vasilets A. V. // Nuovo Cim. A. 1989. V. 102. P. 25.
112. Diakonov D. I. *et al.* // Phys. Rev. D. 1989. V. 39. P. 3509.
113. Goldman T. *et al.* // Mod. Phys. Lett. A. 1998. V. 13. P. 59.
114. Stancu Fl., Pepin S., Glozman L. Ya. // Phys. Rev. D. 1998. V. 57. P. 4393.
115. Glozman L. Ya. // Nucl. Phys. A. 1998. V. 639. P. 65c.
116. Kochelev N. I. // Pisma Zh. Eksp. Teor. Fiz. 1999. V. 70. P. 483; JETP Lett. 1999. V. 70. P. 491.
117. Lichtenberg D. B., Roncaglia R., Predazzi E. // J. Phys. G. 1997. V. 23. P. 865.
118. Gignoux C., Silvestre-Brac B., Richard J. M. // Phys. Lett. B. 1987. V. 193. P. 323.
119. Badalyan A. M., Simonov Yu. A. // Yad. Fiz. 1982. V. 36. P. 1479; Sov. J. Nucl. Phys. 1983. V. 36. P. 860.
120. Kerbikov B. O. // Yad. Fiz. 1984. V. 39. P. 816; Sov. J. Nucl. Phys. 1984. V. 39. P. 516.
121. Morimatsu O., Takizawa M. // Nucl. Phys. A. 1993. V. 554. P. 635.
122. Klebanov I. R., Westerberg K. M. // Phys. Rev. D. 1997. V. 53. P. 2804.
123. Oka M. // Phys. Rev. D. 1988. V. 38. P. 298.
124. Dover C. B. // Nuovo Cim. A. 1989. V. 102. P. 521.
125. Xie S. Q. // J. Phys. G. 1989. V. 15. P. 287.
126. Maltman K. // Nucl. Phys. A. 1989. V. 501. P. 843.
127. Takeuchi S., Nussinov S., Kubodera K. // Phys. Lett. B. 1993. V. 318. P. 1.
128. Donoghue J. F., Golowich E., Holstein B. R. // Phys. Lett. B. 1986. V. 174. P. 441;
Donoghue J. F., Golowich E., Holstein B. R. // Phys. Rev. D. 1986. V. 34. P. 3434.
129. Krivoruchenko M. I., Shchepkin M. G. // Yad. Fiz. 1982. V. 36. P. 1328; Sov. J. Nucl. Phys. 1982. V. 36. P. 769.
130. Baym G. *et al.* // Phys. Lett. B. 1985. V. 160. P. 181.
131. Sanjoy R. Glosch, Phatak S. C. // Phys. Rev. C. 1998. V. 58. P. 1714.
132. Calan C. B., Klebanov I. R. // Nucl. Phys. B. 1985. V. 262. P. 365.
133. Yost S. A., Nappi C. R. // Phys. Rev. D. 1985. V. 32. P. 816.
134. Schaffner-Bielich J. *et al.* // Phys. Rev. C. 1997. V. 55, No. 6. P. 3038–3046.
135. Sakai Ts. *et al.* nucl-th/9912063. 1999.
136. Carroll A. S. *et al.* // Phys. Rev. Lett. 1978. V. 41. P. 777; 1002(E).
137. Condo G. T. *et al.* // Phys. Lett. B. 1984. V. 144.
138. Shakhbazian B. A. *et al.* // Z. Phys. C. 1988. V. 39. P. 151.
139. Shakhbazian B. A. *et al.* // Phys. Lett. B. 1990. V. 235. P. 208.

140. *Shakhbazian B. A. et al.* // Phys. Lett. B. 1993. V. 316. P. 593.
141. *Shakhbazian B. A. et al.* // Nuovo Cim. A. 1994. V. 107. P. 2459.
142. *Aslanian P. Zh. et al.* // JINR Rapid Commun. 1998. No. 1[87].
143. *Aslanian P. Zh. et al.* // Proc. of Intern. Conf. «Bologna-2000», Italy, June 3 – May 29, 2000.
144. *Aslanian P. Zh. et al.* // Nucl. Phys. B. 1999. V. 75B.
145. *Aslanyan P. Zh. et al.* // JINR Commun. E1-2001-265, 2002.
146. *Aslanyan P. Zh. et al.* // Proc. of the 14th Intern. Spin Physics Symp., Osaka, Japan, Oct. 16–21, 2000.
147. *Alekseev A. N. et al.* // Yad. Fiz. 1990. V. 52. P. 1612; Sov. J. Nucl. Phys. 1990. V. 52. P. 1016.
148. *Ejiri H. et al.* // Phys. Lett. B. 1989. V. 228. P. 24.
149. *Longacre R. S. et al.* // Nucl. Phys. A. 1995. V. 590. P. 477c.
150. *Longacre R. S.* // Proc. of the 7th Intern. Conf. on Hadron Spectroscopy, Upton, New York / Eds.: Chung S. U. and Willutzki H. J. AIP Conf. Proc. N. Y., 1998. V. 432. P. 217.
151. *Franklin G. B.* // Nucl. Phys. A. 1986. V. 450. P. 117c.
152. *Iijima T. (BNL E813 Collab.)* // Proc. of the 13th Intern. Conf. on Particles and Nuclei (PAN XII I), Perugia, Italy, June 1993 / Ed. Pascalini A. World Sci., 1994. P. 652.
153. *Barnes P. D.* // Nucl. Phys. A. 1992. V. 547. P. 3c.
154. *Ramsay W. D.* // Proc. of the 14th Intern. Conf. on Particles and Nuclei (PANIC 96) / Ed. C. E. Carlson, J. J. Domingo. World Sci., 1997. P. 602.
155. *Quinn B. et al.* // Proc. of the Intern. Conf. on the Structure of Baryons and Related Mesons, Yale Univ., June 1992 / Ed. Gai M. World Sci., 1993. P. 278.
156. *Stotzer R. W. et al.* // Phys. Rev. Lett. 1997. V. 78. P. 3646.
157. *Yamamoto K. et al.* // Nucl. Phys. A. 1998. V. 639. P. 371c.
158. *May M.* // Ibid. P. 363c.
159. *Rusek A. et al.* // Phys. Rev. C. 1995. V. 52. P. 1580;
Rusek A. et al. // Nucl. Phys. A. 1995. V. 585. P. 59c.
160. *Belz J. et al. (BNL-E888 Collab.)* // Nucl. Phys. A. 1995. V. 585. P. 97c.
161. *Belz J. et al. (BNL-E888 Collab.)* // Phys. Rev. D. 1996. V. 53. P. 3487.
162. *Belz J. et al.* // Phys. Rev. Lett. 1996. V. 76. P. 3277; Phys. Rev. C. 1997. V. 56. P. 1164.
163. *Crawford H. J.* // Nucl. Phys. A. 1998. V. 639. P. 417c.
164. *Chemakin I. et al. (BNL E910 Collab.)* // Ibid. P. 407c.
165. *Paganis S. D. et al.* nucl-ex/9910007.

166. Bassalleck B. *et al.* (BNL E813/E836 Collab.) // *Few-Body Syst. Suppl.* 1995. V.9. P.51.
167. Bassalleck B. // *Proc of the 6th Conf. on Intersections between Part. and Nucl. Phys. Big Sky, Montana, USA / Ed. T.W. Donnelly. Am. Inst. of Phys. AIP Conf. Proc.* 412. N. Y., 1997. P.457.
168. Chrien R. E. // *Nucl. Phys. A.* 1998. V.629. P.388c.
169. Bassalleck B. // *Ibid.* V.639. P.401c.
170. Aokiet S. *et al.* // *Phys. Rev. Lett.* 1990. V.65. P.1729.
171. Imai K. // *Nucl. Phys. A.* 1991. V.527. P.181c.
172. Imai K. // *Nucl. Phys. A.* 1992. V.547. P.199c.
173. Ahn J. K. *et al.* // *Ibid.* P.211c.
174. Ahn J. K. *et al.* // *Nuovo Cim. A.* 1994. V.107. P.2415.
175. Ahn J. K. *et al.* // *Phys. Lett. B.* 1996. V.378. P.53.
176. Ahn J. K. *et al.* (KEK-PS E224 Collab.) // *Nucl. Phys. A.* 1998. V.639. P.379c.
177. Ahn J. K. *et al.* (KEK-PS E224 Collab.) // *Phys. Lett. B.* 1998. V.444. P.267.
178. Imai K. // *Nucl. Phys. A.* 1993. V.553. P.667c.
179. Nakazawa K. // *Nucl. Phys. A.* 1998. V.639. P.345c.
180. Barmin V. V. *et al.* // *Nucl. Phys. A.* 1993. V.558. P.361c.
181. Barmin V. V. *et al.* // *Phys. Lett. B.* 1996. V.370. P.233.
182. Ashery D. // *Hyp. Int.* 1996. V.103. P.253.
183. Alavi-Harati A. *et al.* (KTeV Collab.). hep-ex/9910030.
184. Mitchell J. W. (NA49 Collab.) // *Proc. of Intern. Symp. on Strangeness and Quark Matter / Eds. G. Vassiliadis et al. World Sci., 1995. P.249.*
185. Paul S. (WA89 Collab.) // *Proc. of the 13th Intern. Conf. on Particles and Nuclei (PANXIII) / Ed. A. Pascolini. World Sci., 1994. P.646;*
Povh B. // *Proc. of the U.S.–Japan Seminar on Properties and Interactions of Hyperons / Eds. Gibson B. F., Barnes P. D., Nakai K. World Sci., 1994. P.211;*
Godbersen M. (WA89 Collab.) // *Proc. of the 5th Conf. on Intersections between Part. and Nucl. Phys. St. Petersburg, Florida, USA / Ed. S. J. Seestrom. Am. Inst. of Phys. AIP Conf. Proc. V.338. N. Y., 1995. P.533.*
186. Jacholkowski A. *et al.* (WA97 Collab.) // *J. Phys. G.* 1999. V.25. P.423.
187. Alexander G. *et al.* (OPAL Collab.) // *Phys. Lett. B.* 1996. V.384. P.377.
188. Coffin J. P., Kuhn C. // *J. Phys. G.* 1997. V.23. P.2117.
189. Aerts A. T. M., Dover C. B. // *Phys. Rev. Lett.* 1982. V.49. P.1752.
190. Aerts A. T. M., Dover C. B. // *Phys. Rev. D.* 1983. V.28. P.450.
191. Aerts A. T. M., Dover C. B. // *Phys. Rev. D.* 1984. V.29. P.433.

192. *Dover C. B., Koch P., May M.* // Phys. Rev. C. 1989. V. 40. P. 115.
193. *Sano M., Wakai M., Bando H.* // Phys. Lett. B. 1989. V. 224. P. 359.
194. *Kishimoto T.* // Phys. Rev. Lett. 1989. V. 62. P. 2456;
Kishimoto T. // Nuovo Cim. A. 1989. V. 102. P. 553.
195. *Dover C. B. et al.* // Phys. Rev. C. 1991. V. 44. P. 1636.
196. *Moinester M. A., Dover C. B., Lipkin H. J.* // Phys. Rev. C. 1992. V. 46. P. 1082.
197. *Aizawa N., Hirata M.* // Z. Phys. A. 1992. V. 343. P. 103.
198. *Rotondo F. S.* // Phys. Rev. D. 1993. V. 47. P. 3871.
199. *Cole B. A., Moulson M., Zajc W. A.* // Phys. Lett. B. 1995. V. 350. P. 147.
200. *Bashinsky S. V., Jaffe R. L.* // Nucl. Phys. A. 1997. V. 625. P. 167.
201. *Cousinsand R. D., Klein J. R.* // Phys. Rev. D. 1997. V. 56. P. 1673.
202. *Batty C. J., Friedman E., Gal A.* // Phys. Rev. C. 1999. V. 59. P. 295.
203. *Kahanaand D. E., Kahana S. H.* // Phys. Rev. C. 1999. V. 60. P. 065206.
204. *Danyasz M. et al.* // Phys. Rev. Lett. 1963. V. 11. P. 29;
Danyasz M. et al. // Nucl. Phys. 1963. V. 49. P. 121.
205. *Prowse D. J.* // Phys. Rev. Lett. 1966. V. 17. P. 782.
206. *Aoki S. et al.* // Prog. Theor. Phys. 1991. V. 85. P. 1287.
207. *May M.* // Proc. of the 25th INS Intern. Symp. on Nucl. and Part. Phys. with High-Intensity Proton Accelerators / Ed. Komatsubara T. K., Shibata T., T. Nomura. World Sci., 1998. P. 312.
208. *Dalitz R. H. et al.* // Proc. Soc. Lond. A. 1989. V. 426. P. 1.
209. *Yamamoto Y., Takaki H., Ikeda K.* // Prog. Theor. Phys. 1991. V. 86. P. 867.
210. *Dover C. B. et al.* // Phys. Rev. C. 1991. V. 44. P. 1905.
211. *Tamagaki R.* // Prog. Theor. Phys. 1991. V. 85. P. 321.
212. *Sakai T., Yazaki K., Shimizu K.* // Nucl. Phys. A. 1995. V. 594. P. 247.
213. *Diakonov D., Petrov V., Polyakov M.* // Z. Phys. A. 1997. V. 359. P. 305.
214. *Matheus R. D. et al.* // Phys. Lett. B. 2004. V. 578. P. 323; hep-ph/0309001;
Matheus R. D. et al. hep-ph/0406246.
215. *Jaffe R. L., Wilczek F.* // Phys. Rev. Lett. 2003. V. 91. P. 232003; hep-ph/0307341.
Jaffe R. L., Wilczek F. // Phys. Rev. D. 2004. V. 69. P. 114017; hep-ph/0312369.
216. *Ellis J. et al.* // JHEP. 2004. V. 0405. P. 002; hep-ph/0401127.
217. *Lee Hee-Jung, Kochelev N. I., Ventoa V.* hep-ph/0412127. 2004.
218. *Guzey V.* // Phys. Rev. C. 2004. V. 69. P. 065203; hep-ph/0402060.
219. *Guzey V., Polyakov M.* hep-ph/0501010. 2005.
220. *Glozman L. Ya.* // Phys. Lett. B. 2003. V. 575. P. 18; hep-ph/0308232.

221. Bleicher M. et al. // Phys. Lett. B. 2004. V. 595. P. 595.
222. Letessier J. et al. // Phys. Rev. C. 2003. V. 68. P. 061901.
223. Liu F. M. et al. hep-ph/0404156;
Csikor F. et al. hep-lat/0407033.
Liu M. et al. // Phys. Lett. B. 2004. V. 597. P. 333; hep-ph/0404156.
224. Karliner M., Lipkin H. // Phys. Lett. B. 2004. V. 575. P. 249; hep-ph/0402260.
Karliner M., Lipkin H. // Ibid. V. 594. P. 273; hep-ph/0402008.
225. Hicks K. // Proc. of IX Intern. Conf. on Hypernuclear and Strange Particle Physics, Mainz, Germany, Oct. 2006; hep-ph/0703004.
226. Akers D. hep-ex/0310014. 2004.
227. Arkhipov A. A. hep-ph/0403284v3. 2004.
228. Palazzi P. p3a-2005-005. 2005. <http://particlez.org/p3a/abstract/2005-002.html>
229. Nambu Y. An Empirical Mass Spectrum of Elementary Particles // Prog. Theor. Phys. 1952. V. 7. P. 131.
230. Mac Gregor M. H. // IJMPA. 2005. V. 20, No. 4. P. 719; Addendum // IJMPA. 2005. V. 20, No. 13. P. 2893, and references by the same author therein. <http://particlez.org/p3a/abstract/2005-003.html>
231. Amsler C., Tornqvist N. A. // Phys. Rep. 2004. V. 389. P. 61117.
232. Close F. E., Tornqvist N. A. // J. Phys. G. 2002. V. 28. P. R249.
233. Nakano T. et al. (LEPS Collab.) // Phys. Rev. Lett. 2003. V. 91. P. 012002; hep-ex/0301020;
Barmin V. V. et al. (DIANA Collab.) // Phys. At. Nucl. 2003. V. 66. P. 1715; Yad. Fiz. V. 66;
Stepanyan S. et al. (CLAS Collab.). hep-ex/0307018;
Barth J. et al. (SAPHIR Collab.). hep-ex/0307083;
Kubarovsky V., Stepanyan S. (CLAS Collab.). hep-ex/0307088;
Asratyan A. E., Dolgolenko A. G., Kubantsev V. A. hep-ex/0309042;
Kubarovsky V. et al. (CLAS Collab.). hep-ex/0311046;
Airapetian A. et al. (HERMES Collab.). hep-ex/0312044;
Chekanov S. et al. (ZEUS Collab.) // Phys. Lett. B. 2004. V. 591. P. 2;
Alev A. et al. (SVD Collab.). hep-ex/0401024;
Trojan Yu. et al. JINR, D1-2004-39. Dubna, 2004; hep-ex/0404003. 2004;
Aslanyan P. Zh. et al. hep-ex/0403044. 2004; JINR Commun. E1-2004-137. Dubna, 2004.
234. Kabana S. // 20th Winter Workshop on Nuclear Dynamics «Nuclear Dynamics», Trelawny Beach, Jamaica, March 15–20, 2004;
Kabana S. hep-ph/0501121. 2005.
235. Barmin V. et al. (DIANA Collab.). hep-exp/06003018. 2006; Phys. At. Nucl. 2003. V. 66. P. 1715–1718.

236. *Aleev A. et al.* SVD-2 Experiment // Proc. of ICHEP06, Moscow, July 29, 2006; hep-ex/0509033. 2005.
237. *Kubarovsky A. et al.* // Proc. of ICHEP, Moscow, July 29 – Aug. 2, 2006; Part. Nucl., Lett. 2002. No. 5[114].
238. *Troyan Yu. A. et al.* JINR Commun. E1-2002-214. Dubna, 2002.
239. *Colangelo G., Gasser J., Leutwyler H.* // Nucl. Phys. B. 2001. V. 603. P. 125; *Aitala E. M. et al. (E791 Collab.)* // Phys. Rev. Lett. 2002. V. 89. P. 121801; hep-ex/0204018.
240. *Ablitim M. et al. (BES Collab.)* // Phys. Lett. B. 2004. V. 598. P. 149; hep-ex/0406038.
241. *Bugg D. V.* // Eur. Phys. J. A. 2005. V. 25. P. 107; Erratum // Ibid. 2005. V. 26. P. 151; hep-ex/0510026.
242. *Blobel V. et al.* DESY 73/51. 1973. P. 151; hep-ex/0510026.
243. *Bochmann K. et al.* // Nucl. Phys. B. 1980. V. 166. P. 284.